A NEURAL MODEL OF CEREBELLAR LEARNING FOR ARM MOVEMENT CONTROL: CORTICO-SPINO-CEREBELLAR DYNAMICS

J.L. Contreras-Vidal†, Stephen Grossberg‡, and Daniel Bullock‡

Department of Cognitive and Neural Systems
and
Center for Adaptive Systems
Boston University
677 Beacon Street
Boston, Massachusetts 02215 ¶

Key words: cerebellum, learning, arm movement, spinal cord, motor cortex, neural model

Running head: Cerebellar Learning for Arm Movement Control

Send all communications concerning the manuscript and requests for reprints to:

Professor Stephen Grossberg
Boston University
Department of Cognitive and Neural Systems
and Center for Adaptive Systems
677 Beacon Street
Boston, MA 02215
Phone: (617) 353-7857, Fax: (617) 353-7755
Email: steve@cns.bu.edu

Abstract

A neural network model of opponent cerebellar learning for arm movement control is proposed. The model illustrates how a central pattern generator in cortex and basal ganglia, a neuromuscular force controller in spinal cord, and an adaptive cerebellum cooperate to reduce motor variability during multi-joint arm movements using mono- and bi-articular muscles. Cerebellar learning modifies velocity commands to produce phasic antagonist bursts at interpositus nucleus cells whose feedforward action overcomes inherent limitations of spinal feedback control of tracking. Excitation of α motoneuron pools combined with inhibition of their Renshaw cells by the cerebellum facilitate movement initiation and optimal execution. Transcerebellar pathways are opened by learning through long-term depression (LTD) of parallel fiber-Purkinje cell synapses in response to conjunctive stimulation of parallel fibers and climbing fiber discharges that signal muscle stretch errors. The cerebellar circuitry also learns to control opponent muscles pairs, allowing co-contraction and reciprocal inhibition of muscles. Learning is stable, exhibits load compensation properties, and generalizes better across movement speeds if motoneuron pools obey the size principle. The intermittency of climbing fiber discharges maintains stable learning. Long-term potentiation (LTP) in response to uncorrelated parallel fiber signals enables previously weakened synapses to recover. Loss of climbing fibers, in the presence of LTP, can erode normal opponent signal processing. Simulated lesions of the cerebellar network reproduce symptoms of cerebellar disease, including sluggish movement onsets, poor execution of multi-joint plans, and abnormally prolonged endpoint oscillations.

1   Introduction

Clinical and experimental data on both oculomotor and skeletomotor systems suggest that an intact cerebellum is necessary for learning and performance of accurate, rapid movements, especially movements involving multiple degrees of freedom (DOFs). Systems with multiple, mechanically-linked DOFs are hard to control because the inertial, gravitational, and interaction forces, which must be compensated whenever they do not assist desired motion or stasis, are configuration- and rate-dependent. In very slow movements, there can be sufficient time to use sensory feedback to adjust motor commands before errors caused by uncompensated forces can grow very large. But as movement speeds increase, feedback begins to arrive too late to be useful for on-line control of the current movement. In such cases, accuracy can not be guaranteed unless motor commands to entire groups of muscles can be accurately timed and scaled prior to the arrival of feedback.

Such considerations, in combination with observations regarding the cerebellum's typical "side-loop" embedding (Ito, 1984 and Figure 1) within the sensory-motor system, support a view of the cerebellum as an adaptive controller capable of calibrating parallel feedforward motor commands that can substitute for slow feedback-based commands and thereby enable high speed and accuracy without iterations (Grossberg and Kuperstein, 1986). Relatedly, the cerebellum has been viewed by some as an adaptive calibrator of internal forward models that allow computation of the expected effects of motor commands (Kawato and Gomi, 1991; Miall, Malkmus, and Robertson, 1996). This application of a cerebellar side-loop would allow substitution of fast, "internal feedback" for slow, sensor-based feedback. These two views are not incompatible (Stein and Glickstein, 1992). In both perspectives, the cerebellum learns to substitute a faster, anticipatory process for a slower, reactive one. Also compatible with both approaches is the hypothesis that external feedback, although rendered progressively less important for on-line control as cerebellar learning progresses, retains a critical teaching role; such feedback is ultimately the only reliable source of information regarding the adequacy of the timing and scaling of feedforward movement commands, or of internal model calibration. At the level of the cerebellar system, these approaches thus postulate that feedback error signals in motor coordinates are converted by the inferior olive into discrete teaching signals, which guide incremental, trial-by-trial adjustments in the cerebellar adaptive weights that control anticipatory actions.

Though supported by a wealth of data, the view of the cerebellum as an adaptive controller capable of using feedback to learn how to substitute a faster for a slower "solution" in repeatable task contexts has not gone unchallenged. Brainstem and spinal cord circuitry apparently provide some basis for task-specific recruitment and control of muscle synergies, and experimental studies of decerebrate/decerebellate animals have produced evidence suggesting that such circuitry has some of the same associative competence widely attributed to the cerebellum (Bloedel and Bracha, 1995). Though suggestive of partial redundancy, such studies have not shown that the brainstem/spinal circuitry affords a large, content-addressable memory for learning and storage of the relatively arbitrary task contexts and action groupings required for a large repertoire of learned skills. Nor has it been shown that such circuitry is capable of learning to generate novel movements whose accurate performance requires that different synergists (DOFs) be activated at different times after
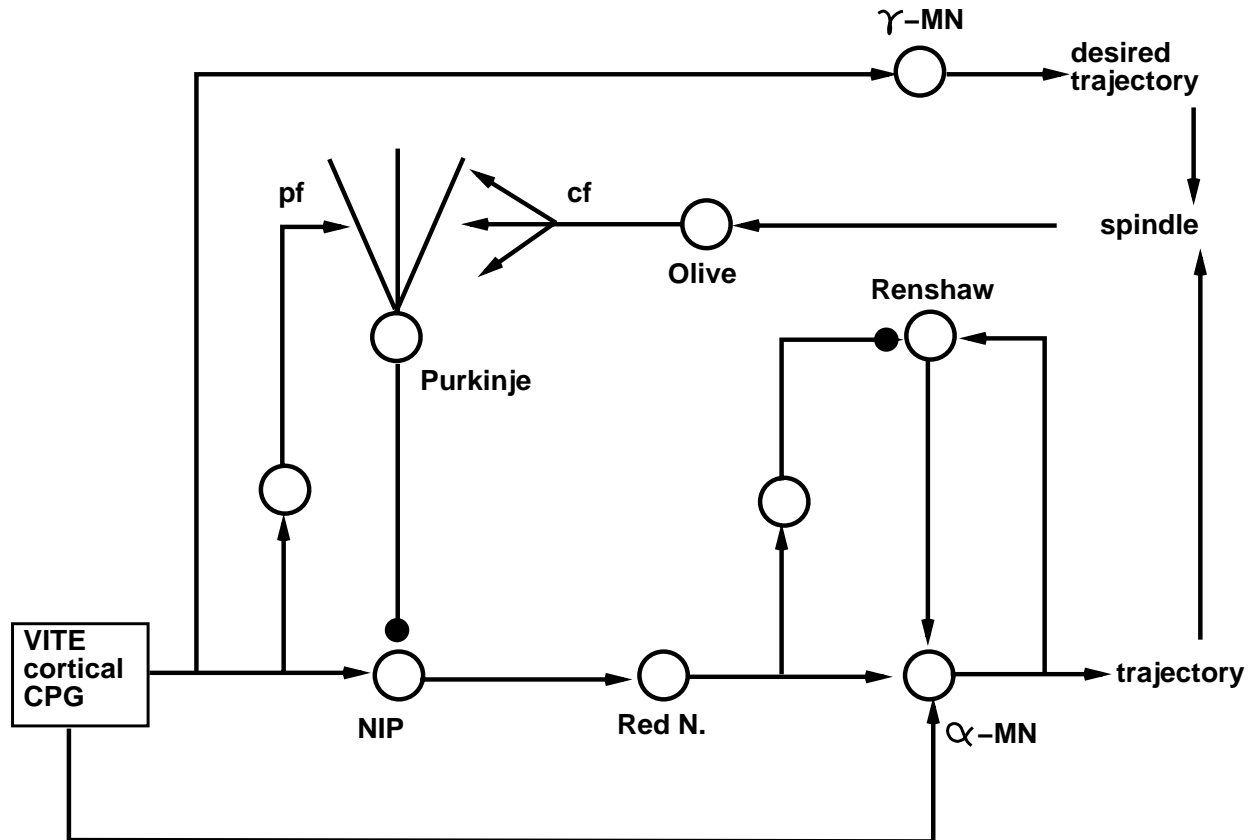
Figure 1: Cortico-spino-cerebellar model structure: Excitatory pathways from a central pattern generator (VITE) send velocity commands to motoneurons in the spinal cord as well as mossy fiber collaterals which may bifurcate and send branches to both the cerebellar cortex and nuclei. The deep cerebellar nuclear cells ultimately project through the red nucleus to motoneurons and spinal interneurons such as Renshaw cells. Spindle error signals resulting from a comparison of the desired with the actual trajectory project to motoneurons (not shown) and to the inferior olive, where they act as teaching signals via climbing fibers to the Purkinje cells. These teaching signals regulate long-term depression (LTD) at synapses where active parallel fibers contact Purkinje cells. It is hypothesized that for purposes of stability and economy of effort the path for velocity commands through the cerebellum is normally closed by Purkinje inhibition of nuclear cells, while the gain of excitatory signals through the motoneuron stage (both from descending commands and from proprioceptive reflexes) is low due to Renshaw inhibition of alpha motoneurons. However, LTD opens the gate in the transcerebellar sidepath and allows transient commands to simultaneously excite motoneurons and inhibit Renshaw cells. Keys: CPG, central pattern generator; NIP, nucleus interpositus cells; pf, parallel fibers; cf, climbing fibers; γ-MN, gamma motoneurons; α-MN, alpha motoneurons; arrow terminated pathways are excitatory; filled-circle terminated paths are inhibitory.

detection of a context stimulus. By contrast, several features of cerebellar architecture and dynamics qualify it as the best known candidate for such a sensory-motor memory: the cerebellum's side-loop embedding, the large-scale projection of state-specifying afferents to the granule cell layer of the cerebellar cortex, the further fanout from granule cells of the parallel fibers (PFs), and the long-term plasticity of PF-Purkinje synapses – now demonstrated both in vitro and in vivo (e.g., Crepel, Hemart, Jaillard, and Daniel, 1996). Moreover, recent modeling studies indicate how the specialized biochemistry of Purkinje cells, in particular the slowly developing calcium responses of the metabotropic glutamate receptor cascade, can allow the cerebellum to learn timed sequences of motor control signals (Fiala and Bullock, 1996; Fiala, Grossberg, and Bullock, 1996; Kano, 1996).

Analysing the distinct functions of elements of the cerebellar system requires systematic modeling and simulations. By this we mean simulations in which the model cerebellar system includes all the major cell types; the model cerebellum's afferent signals are generated by simulated receptors and circuits that are part of the simulation; and its efferent signals affect the simulated motor plant via a simulated spinal circuit. In such a model, all major elements of the cerebellar system can be examined for their contribution, if any, to improved operation of a sensory-motor system whose dynamics are realistic enough to appropriately challenge cerebellar provisions for learning, memory, and performance. This report describes such a model, with a focus on how the cerebellar-olivary side-loop can exert learned control of opponently organized limb spinal circuits, and thereby improve the performance of rapid two-joint movements, whose desired form is determined by output from a central pattern generator.

Because the cerebellar model interacts with a two-joint limb moved by sets of opponent muscles, the simulations are pertinent to issues of opponency both within the cerebellar system and in the descending pathways from cerebellum to the spinal cord. Regarding the latter, there has been great interest in recent years in the role of the red nucleus (RN) of the reticular formation and the associated cerebello-rubro-spinal pathway. In many vertebrates, this pathway is a key element in the system for voluntary movement, and its analysis promises to illuminate cerebellar function because the magnocellular division of the RN is dominated by inputs from the nucleus interpositus (NIP) of the cerebellum (e.g., Robinson, Houk and Gibson, 1987). Much prior modeling work has focused on the role of the NIP/RN in eye blink conditioning (e.g., Bartha, Thompson, and Gluck, 1991; Fiala, Grossberg, and Bullock, 1996). The comprehensive skeletomotor simulation strategy followed here refines and elaborates prior treatments of the limb-control role of the cerebello-rubro-spinal pathway. Our simulations show a strong advantage, within the opponent muscle system, of the reported dual action – alpha-motoneuron excitation with Renshaw cell inhibition (Henatch, Meyer-Lehman, Windhorst, and Schmidt, 1986) – of descending signals from the NIP/RN.

Because the cerebellar cortex model included all major cell types, as well as the interactions implied by their connectivity and sign of action, the results illustrate how interactions in cerebellar cortex may assist rapid switching between the NIP zones that alternately activate opponent muscles during rapid joint rotations. Such rapid switching appears to be necessary for appropriate shaping of the motor command pulses needed to achieve desired acceleration and deceleration of limbs. Taken together with prior results regarding adaptive timing, these results clarify how the cerebellum can contribute to generation of

critically timed and shaped, multi-phasic, burst patterns, which are exhibited by muscles during rapid movement in normal animals, but which are disordered during cerebellar deactivation (Hore, Wild, and Deiner, 1991).

The third aspect of our results concerns learning. The model includes a local circuit for signal processing by the olivary nucleus. Its inclusion allowed a demonstration that there is no incompatibility between data indicating that the olive is inherently oscillatory (Llinás, 1989) and the hypothesis that the olive's output via climbing fibers constitutes a discrete error-feedback driven teaching signal. The results also show that the climbing fiber signals produced by the olivary model are suitable for regulating incremental weight adjustments in the cerebellar cortex. In the case studied here, PF-Purkinje cell synapses exhibit both LTD and LTP, depending upon whether PF activations do or do not correlate with climbing fiber activations of Purkinje cells (Sakurai, 1987). We have elsewhere extended the present learning concept to model how the metabotropic glutamate receptor system can enable LTD at the PF-Purkinje cell synapses to adaptively time depression of Purkinje cell firing. This event enables subcortical pathways to read out appropriately timed learned movement gains (Fiala, Grossberg, and Bullock, 1996). Because of the opponent form of the model, these learning results also reveal that muscle opponency imposes no constraints on prewiring at the level of the cerebellar cortex other than the constraint that CFs carrying signals of errors from opponent muscle channels should project to distinct parasaggital microzones (Ito, 1984). Some aspects of this work have been briefly reported in Bullock, Contreras-Vidal, and Grossberg, (1993a, 1993b) and in a dissertation (Contreras-Vidal, 1994).

2   Methods

Figure 1 schematizes the components needed to model the cerebellar system as it is embedded within the reaching control system that we studied. But it also exemplifies the typical embedding, in which there exists some primary generator of movement, such as a reflex circuit, a locomotor pattern generator, a saccade generator, etc., which sends projections to motoneurons but also to the cerebellum. The cerebellum in turn sends a projection to the same motoneurons that are addressed by the pattern generator. In addition, there is a feedback signal pathway to one of the olivary nuclei, typically an error feedback signal such as retinal slip, muscle stretch, unexpected contact, or a signal reporting compensatory action by an error-feedback-driven motor command generator. The cerebellum is thus part of a side-loop with respect to the direct projection from primary generator to motoneurons, and the side-loop circuit receives teaching signals generated by residual errors of movement.

The Figure 1 system is shown in greater detail in Figure 2. As the kinematic central pattern generator (CPG), we chose the VITE model (Bullock and Grossberg, 1988), which embodies key properties of the voluntary, and largely cortical, arm trajectory generation network that outputs to lower brain centers through area 4 (Bullock, Cisek, and Grossberg, 1997). The VITE CPG generates desired position and desired velocity commands. As the spinal recipient of commands from both the VITE CPG and the cerebellum, we chose the FLETE model (Bullock and Contreras-Vidal, 1993; Bullock and Grossberg, 1988,
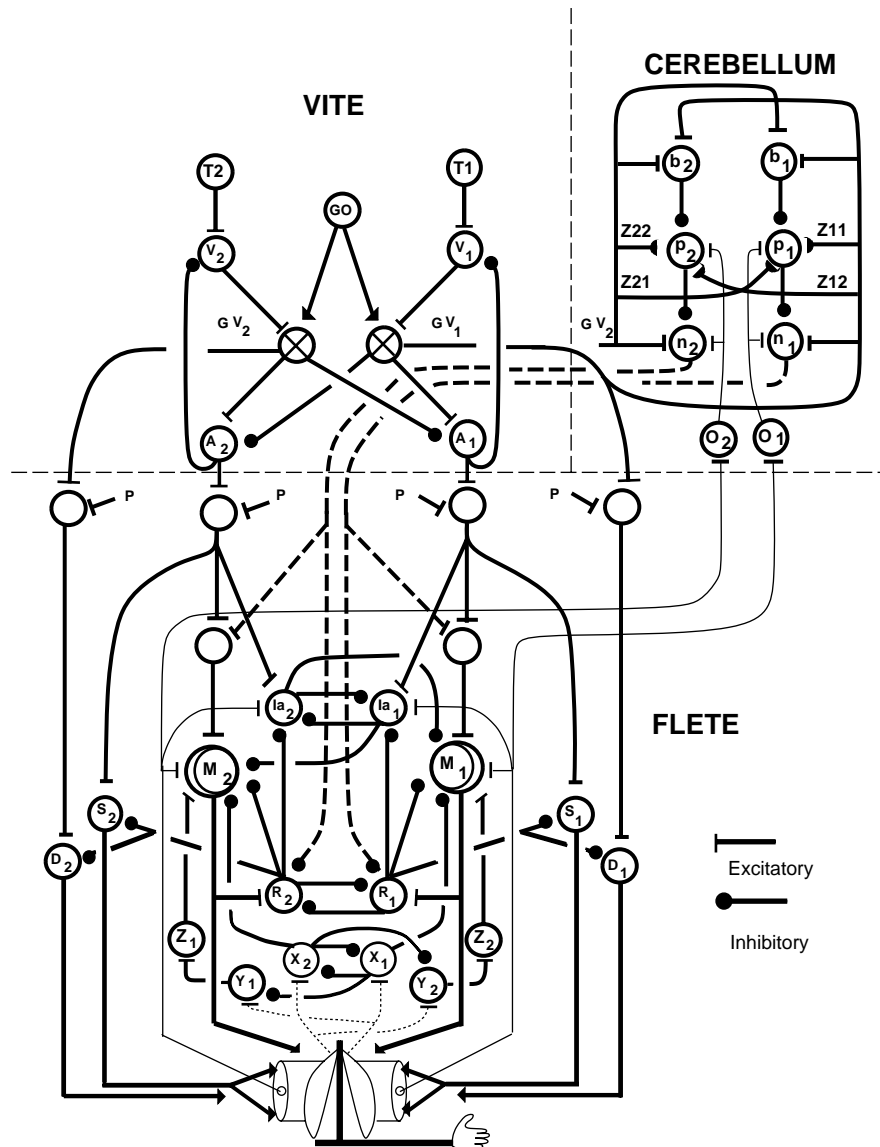
Figure 2: Neural network representation of the neuromuscular control system including feedforward cerebellar control. Upper-left part: The VITE model for variable-speed trajectory generation. Lower part: The FLETE model of the opponently organized spinomuscular system. Dotted lines show feedback pathways from sensors embedded in muscles. The two lateral feedback pathways arise in spindle organs sensitive to muscle stretch and its first derivative. The two medial feedback pathways arise in Golgi tendon organs sensitive to muscle force. Signals A_1 and A_2 specify the desired position vector, and the signals $V_1 G$ and $V_2 G$ specify the desired velocity vector; signals T_1 and T_2 specify the target position vector; signal P scales the level of coactivation, and signal GO scales speed of movement. Upper-right part: Feedforward cerebellar model computes transient inverse-dynamic signals that excite motoneurons and modulate the gain in spinal circuits. Key: B, basket cell; p, Purkinje cells; n, nucleus interpositus cells; O, inferior olive; CF, climbing fibers; z, long-term memory weights. Paths terminated by filled dots are inhibitory; all others are excitatory.

1991, 1992), an opponent muscle control model of how spinal circuits afford independent voluntary control of joint stiffness and joint position. This model incorporates second order dynamics, which play a large role in realistic limb movements.

The model's name is an acronym for Factorization of LEnth and TEnsion, which summarizes the most important design principle used to explain why the spinal circuitry e-volved to its modern form. For all aspects of motor control, it is critical that the higher nervous system be able to exercise independent control over muscle length and the force or tension developed at that muscle length. The following system of equations describes a subset of the spinal circuitry that can provide this independent control property in a robust way.

The scenario for the simulation studies can be described with reference to Figure 1. Entering on the left is a velocity command (output by the VITE CPG, detail in Figure 2), which is projected to both cerebellar cortex and to a deep cerebellar nuclear site, here interpreted as a zone within the nucleus interpositus or NIP (Martin and Ghez, 1991; Gibson, Houk, and Kohlerman, 1985). The NIP projects to and dominates the Red nucleus (RN), which in turn excites alpha motoneurons and inhibits associated Renshaw cells (Henatch *et al.*, 1986). However, excitation of motoneurons by this pathway is prevented by Purkinje inhibition of NIP unless PF-signaled contexts from the CPG and spino-muscular system have reliably led to teaching signals from the olive that have induced PF-Purkinje LTD and thereby transiently reduce Purkinje inhibition of the NIP, as has been demonstrated for the analogous case of eye-blink conditioning (reviewed in Bullock, Fiala, and Grossberg, 1994). The right side of the diagram shows that one proposed teaching signal derives from feedback from muscle spindle organs. Experiments on the stretch reflex (e.g., Matthews, 1981) have demonstrated that muscle spindles normally signal the discrepancy (or error) between an intrafusal muscle length setting and the actual extrafusal length. Such discrepancies would also arise naturally during voluntary movement, under conditions of alpha-gamma coactivation by a descending desired kinematics signal, if the rate of limb movement/joint rotation either undershoots or overshoots the desired rate. In summary, to model cerebellar contributions to rapid arm movements, we treat the deep nuclear stage as a normally closed gate which, after learning in particular contexts, will be transiently opened by timed Purkinje cell pausing whenever those contexts recur.

We now present a mathematical specification of the model used to simulate this scenario. The equations used to specify the model mathematically can be divided into three sets: the CPG (VITE) equations, the spino-muscular circuit (two-joint FLETE model) equations, and the cerebellar system equations. Because the first two sets of equations are not a focus of this report, they are introduced with just enough detail to achieve a self-contained exposition. They define the system that is to be assisted by the model cerebellum, which is of primary concern. On the other hand, Tables 1 and 2 summarize neurobiological evidence for each one of the processing stages of the VITE and FLETE models.

Central pattern generator: VITE model

The VITE circuit (Bullock and Grossberg, 1988) is a multi-channel central pattern generator capable of generating desired arm movement trajectories by smoothly interpolating between initial and final length commands for the synergetic muscles that contribute to a prescribed multijoint movement. The rate of the interpolation, and thus the velocity of

movement, is controlled by the product of two signals: a difference vector (DV), which continuously measures the residual vector of muscle length changes needed to reach the final position, and a volitional gating signal, called the GO signal. As shown in the upper part of Figure 2, the DV with components V_1 and V_2 is computed in the CPG by subtracting an outflow present position vector (PPV) command with components A_1 and A_2 from a target position vector (TPV) command with components T_1 and T_2. These relationships lead to the following system.

Model element	Cell type by physiology	References
Desired velocity vector (DVV)	area 4 phasic movement-time (MT)	Fromm, Wise, & Evarts, 1984; Georgopoulos, Kalaska, Caminiti, & Massey, 1982 Kalaska, Cohen, Hyde, & Prud'homme, 1989
Present position vector (PPV)	area 4 tonic	Fromm, Wise, & Evarts, 1984; Kalaska, Cohen, Hyde, & Prud'homme, 1989; Kettner, Schwartz, & Georgopoulos, 1988
Difference vector (DV)	posterior area 5 phasic	Burbaud, Doegle, Gross, & Bioulac, 1991; Chapman, Spidalieri, & Lamarre, 1984; Crammond & Kalaska, 1989; Kalaska, Cohen, Prud'homme, & Hyde, 1990; Lacquaniti, Guigon, Bianchi, Ferraina, & Caminiti, 1995
Target position vector (TPV)	area 5 or area 7b	Lacquaniti, Guigon, Bianchi, Ferraina, & Caminiti, 1995; Anderson, 1987; Robinson & Burton, 1980; Dum & Strick, 1990
GO signal	globus pallidus	Horak & Anderson, 1984a; Horak & Anderson, 1984b; Kato & Kimura, 1992

Table 1: Proposed correspondence between VITE model elements and brain elements

GO signal dynamics are defined by the sigmoidal functions

$$G(t) = G_0 \frac{(t - \mathcal{T}_i)^2}{.5 + (t - \mathcal{T}_i)^2} u[t - \mathcal{T}_i], \tag{1}$$

where parameter G_0 scales the GO signal, $\mathcal{T}_i$ is the onset time of the ith volitional command, and $u[t]$ is a step function that jumps from 0 to 1 to initiate movement. Difference vector dynamics are defined by

$$\frac{d}{dt} V_i = 30(-V_i + T_i - A_i), \tag{2}$$

where T_i is the target position command for muscle channel i, i=1, 2, and A_i is the present position command. The difference vector activities (V_i, V_j) are half-wave rectified to generate output signals $[V_i]^+$ and $[V_j]^+$ to the next processing stage, where Figure 2 shows that they are multiplied, or gated, by the GO signal to form the vector $(G[V_i]^+, G[V_j]^+)$. This vector is called the desired velocity vector (DVV) because opponent subtraction of

its output signals determine the rate of change of the PPV at the next processing stage:

Connection Type	Citations
$\alpha\text{-}MN_i \overset{+}{\rightarrow} R_i$	Renshaw (1941; 1946) Eccles, Fatt & Koketsu (1954)
$R_i \overset{-}{\rightarrow} \alpha\text{-}MN_i$	Renshaw (1941) Eccles, Fatt & Koketsu (1954)
$R_i \overset{-}{\rightarrow} IaIN_i$	Hultborn, Jankowska & Lindström (1971)
$R_i \overset{-}{\rightarrow} \gamma\text{-}MN_i$	Ellaway (1968) Ellaway & Murphy (1980)
$R_i \overset{-}{\rightarrow} R_j$	Ryall(1970) Ryall & Piercey (1971)
$IaIN_i \overset{-}{\rightarrow} \alpha\text{-}MN_j$	Eccles & Lundberg (1958) Araki, Eccles & Ito (1960)
$IaIN_i \overset{-}{\rightarrow} IaIN_j$	Eccles & Lundberg (1958) Hultborn, Jankowska & Lindström (1971) Hultborn, Illert & Santini (1976) Baldiserra *et al.* (1987)
$Ia_i\ fiber \overset{+}{\rightarrow} IaIN_i$	Hultborn, Jankowska & Lindström (1971) Baldiserra *et al.* (1987)
$Ia_i\ fiber \overset{+}{\rightarrow} \alpha\text{-}MN_i$	Lloyd (1943)
$IbIN_i \overset{-}{\rightarrow} \alpha\text{-}MN_i$	Laporte & Lloyd (1952) Eccles, Eccles & Lundberg (1957) Kirsch & Rymer (1987)
$IbIN_i \overset{+}{\rightarrow} \alpha\text{-}MN_j$	Laporte & Lloyd (1952) Eccles, Eccles & Lundberg (1957)
$IbIN_i \overset{-}{\rightarrow} IbIN_j$	Laporte & Lloyd (1952) Eccles, Eccles & Lundberg (1957) Brink, Jankowska, McCrea & Skoog (1983)
non-specific $P \overset{+}{\rightarrow}$ spinal motor pools	Humphrey & Reed (1983) DeLuca (1985)

Table 2: Evidence for connectivity and physiology incorporated in FLETE

$$\frac{d}{dt}A_i = G[V_i]^+ - G[V_j]^+, \tag{3}$$

where $\{i,j\} = \{1,2\}$ designate opponent muscle commands. By equation (3), the PPV integrates the product of opponent GO times DV signals. These equations treat a case where there are are no cerebellar inputs to the CPG, but this need not always be the case.

Prior studies (Bullock and Grossberg, 1988, 1991) have demonstrated that the VITE equations can be used to explain a large number of robust kinematic features of voluntary point-to-point movements including smooth, bell-shaped velocity profiles, voluntary speed

control that leaves direction and amplitude nearly invariant, peak velocity and acceleration as a function of movement duration, and a Fitts-type speed-accuracy trade off. The model's prediction of duration-dependent velocity profiles has been experimentally verified (Nagasaki, 1989). Recently, the cell types and connectivity of a self-consistently extended version of the VITE model have been used to simulate neuro-physiological data on six identified cell populations in motor and parietal cortex during a variety of movement tasks (Bullock, Cisek, and Grossberg, 1997; Cisek, Grossberg, and Bullock, 1996). This model extension uses proprioceptive feedback to adjust perceived position estimates when obstacles are encountered, and to compensate for static forces. The processing stages used in the present simulations are shown in Table 1. Also, it has been shown recently how basal ganglia structures can generate a time-varying gating signal that has the properties of the GO signal in the VITE model (Contreras-Vidal and Stelmach, 1995).

Opponent spino-muscular circuit: FLETE model with cerebellar inputs

This part of the model, shown in the lower part of Figure 2, incorporates an opponent force generating circuit that (a) attempts to implement the CPG movement commands, (b) measures movement errors and returns error signals on a muscle-by-muscle basis when execution is imperfect, and (c) is modulated by descending cerebellar outputs. As shown in Table 2, the FLETE model equations are based on the known neuroanatomy and physiology of the spino-muscular circuits, which include neural, muscular, and sensory parts.

The model's name is an acronym for Factorization of LEnth and TEnsion, which summarizes the most important design principle used to explain why the spinal circuitry evolved to its modern form. For all aspects of motor control, it is critical that the higher nervous system be able to exercise independent control over muscle length and the force or tension developed at that muscle length. The following system of equations models a subset of the spinal circuitry that can provide this independent control property in a robust way.

The quadratic force-length relationship of muscle is approximated in the model by

$$F_i = k \left([L_i - ,_i + C_i]^+ \right)^2, \tag{4}$$

where indices $i = \{1, 2\}$ designate antagonist muscle pairs, F_i is muscle force, L_i is muscle length, $,_i = 20.9$ is resting muscle length, and C_i is muscle contractile state, thus an activation level, not a length variable. The scaling parameter k was fixed at a value of 1 in the current simulations. The contractile state dynamics are defined by

$$\frac{d}{dt}C_i = \beta_i \left[(B_i - C_i)M_i - C_i \right] - [F_i - ,_F]^+, \tag{5}$$

where the force threshold $,_F = 1$, M_i is α-MN pool activity in muscle control channel i, β_i is contractile rate, and B_i measures the number of contractile fibers. The origin-to-insertion muscle lengths for opponent mono-articular muscles depend on joint angle Θ as follows:

$$L_1 = \sqrt{(cos\Theta)^2 + (20 - sin\Theta)^2} \tag{6}$$

and

$$L_2 = \sqrt{(cos\Theta)^2 + (20 + sin\Theta)^2}. \tag{7}$$

Equations (6) and (7) indicate that a change of joint angle always implies a length increment in one muscle and a length decrement in its opponent. Limb dynamics for a single joint are specified by

$$\frac{d^2}{dt^2}\Theta = \frac{1}{I_m}(F_1 - F_2 + F_e - n\frac{d}{dt}\Theta), \tag{8}$$

where F_e represents an external force, F_i is the force associated with muscle i, $\frac{d}{dt}\Theta$ is angular velocity in radians, I_m is the moment of inertia (set to 1 unless specified otherwise), and n is the joint viscosity coefficient (which is used here at a value that allows it to stand in lieu of muscle-related damping; e.g., that due to the force-velocity characteristic of muscle). The model shows qualitatively similar behavior over a range of viscosities n spanning at least $.1 \leq n \leq .3$.

Both contraction rate and the number of contractile fibers are known to increase with excitatory input to the alpha mononeuron population, among other factors. This is the *size principle* of motor unit organization (Hennemann, 1957, 1985). Accordingly, contraction rate in (5) depends on the level of excitatory input to the alpha motoneuron according to

$$\beta_i = .05 + .01(A_i + n_i + P + E_i), \tag{9}$$

where A_i is the descending present position command, P is a coactivation signal (set equal to 0.3 unless specified otherwise), E_i is stretch feedback from spindles, and n_i is the activity of the NIP/RN zone associated with muscle i. Likewise, the number of contractile fibers recruited into force production also depends upon the net excitatory drive to the alpha motoneuron:

$$B_i = .3 + 3(A_i + n_i + P + E_i). \tag{10}$$

Figure 2 shows that axons emerging form motoneuron pools M_i send excitatory collaterals to Renshaw cells. The Renshaw population activity is modeled by the membrane equation

$$\frac{d}{dt}R_i = (5B_i - R_i)z_iM_i - R_i(.8 + R_j + 25n_i), \tag{11}$$

where the Renshaw cell recruitment rate z_i depended on the level M_i of alpha motoneuron (MN) activation:

$$z_i = .05(1 + M_i). \tag{12}$$

The Renshaw population output signal is

$$R_i^+ = Max[0, R_i], \tag{13}$$

which equals R_i since $R_i \geq 0$ by (11). The alpha MN population activity is also governed by a membrane equation, as are all subsequent model neural populations. Here

$$\frac{d}{dt}M_i = (\lambda B_i - M_i)(A_i + n_i + P + E_i + Z_j^+) - (M_i + 1.6)(0.2 + R_i + X_i + I_j^+), \tag{14}$$

where X_i is the IbIN force feedback (see equation (18)) and Z_j^+ is a signal dependent on the rate of change of IbIN force feedback in the opponent muscle channel (see equation (20)). The alpha MN population output signal is

$$M_i^+ = Max[0, M_i]. \tag{15}$$

Equations (14) and (11) say that descending signals n_i from the NIP/RN have an excitatory effect on alpha MNs and an inhibitory effect on Renshaw cells, as reported by Henatsch *et al.,* (1986). The IaIN population activity is defined by

$$\frac{d}{dt}I_i = (10 - I_i)(A_i + P + E_i) - (I_i + 1)(1 + R_i + I_j^+) \tag{16}$$

and its output signal is

$$I_i^+ = Max[0, I_i] \tag{17}$$

These equations indicate that model IaINs are reciprocally inhibitory (Hultborn, Jankowska and Lindström, 1971) and are not directly affected by descending signals from the NIP/RN. They are, however, indirectly affected by NIP/RN inhibition of Renshaw cells. The net effect is disinhibition of the IaIN associated with an NIP/RN-activated muscle channel. This effect allows signals from NIP to reinforce reciprocal inhibition.

The IbIN population activity is excited by pathways originating in force-sensitive Golgi tendon organs:

$$\frac{d}{dt}X_i = .2(5 - X_i)F_i - X_i(.8 + 0.2X_j). \tag{18}$$

Two other Golgi tendon organ feedback-related activities are a force-derivative related activity:

$$\frac{d}{dt}Y_i = .2(5 - Y_i)F_i - Y_i(1 + X_i) \tag{19}$$

and an interneuron population activity:

$$\frac{d}{dt}Z_i = .2(5 - Z_i)Y_i - Z_i \tag{20}$$

This population's output signal is

$$Z_i^+ = Max[0, Z_i - .2]. \tag{21}$$

Equations (19)–(21) and (14) say that the spinal network computes the derivative of force in one channel, delays it, thresholds it, and then uses the resultant signal to excite alpha MN's in the opponent channel. Such an operation helps brake rapid movements and allows the network to exhibit an inverse myotatic reflex (Bullock, Contreras-Vidal, and Grossberg, 1993c).

The static gamma MN activity is

$$\frac{d}{dt}S_i = 5(2 - S_i)(A_i + P) - (S_i + 1.2)(.2 + .3h(R_i)), \tag{22}$$

where $h(w) = \frac{w}{0.3+w}$, and its output signal is:

$$S_i^+ = Max[0, S_i]. \tag{23}$$

The intrafusal muscle contraction associated with static gamma MN activation obeys:

$$\frac{d}{dt}U_i = (2 - U_i)S_i^+ - U_i \tag{24}$$

The dynamic gamma MN activity satisfies:

$$\frac{d}{dt}D_i = (8 - D_i)(100G[V_i]^+ + P) - (D_i + 1.2)(1 + 100G[V_j]^+ + .5h(R_i)) \tag{25}$$

and its output signal is

$$D_i^+ = Max[0, D_i]. \tag{26}$$

The intrafusal muscle contraction associated with dynamic gamma MN activation is:

$$\frac{d}{dt}N_i = .1(2 - N_i)D_i^+ - 10N_i \tag{27}$$

The spindle receptor activation was modeled with

$$\frac{d}{dt}W_i = (2 - W_i)([U_i + L_i - , _i]^+ + G_v([N_i + \frac{d}{dt}L_i]^+)^{.3} - 10W_i, \tag{28}$$

where $G_v = 2$, and the resting length $, _i = 20.9$ for these simulations. The stretch feedback signal was a linear function of spindle receptor activation

$$E_i = G_s W_i, \tag{29}$$

where feedback gain G_s was set equal to 1.

The 2D planar arm simulations used joint receptor feedback from the shoulder joint. For reasons described later, it was assumed that joint receptors activated by shoulder flexion would project only to alpha motoneuron pools that control elbow flexion, and that only those joint receptors activated by shoulder extension would project to α-MNs that control elbow extension.

The shape of joint receptors' response functions seems to vary from joint-to-joint (see Burgess *et al.*, 1982). For example, elbow and wrist joint receptors discharge primarily near to the end of the joint range (Millar, 1975; Tracey, 1979); but those in the hip signal over a large fraction of the working range of this joint (Carli *et al.*, 1979). In addition, there are articular receptors that do not distinguish between joint flexion or extension, whereas others show responses over roughly half of the joint's range.

Consistent with experimental data (Millar, 1975; Tracey, 1979) on half-range recep-

tors that fire more strongly as extremes are approached, we modeled the joint receptor's dependence on joint angle in (8) with

$$J_f = .75\Theta^{1.3} \; if \; \Theta > 0 \; rad \qquad (30)$$

for shoulder flexion relative to the "zero" angle in the middle of the joint's range and

$$J_e = .75|\Theta|^{1.3} \; if \; \Theta < 0 \; rad \qquad (31)$$

for joint receptors activated by shoulder extension relative to the midpoint.

This two-component neural feedback signal specifies joint angle under both static and dynamic (motion) conditions regardless of direction or speed of angular changes. The signal is bounded because of biomechanical limits on the range of joint angle Θ. For the 2D simulations, the shoulder joint receptor feedback from the agonist and the antagonist channels was used as additional excitatory inputs to the agonist and antagonist α-MN equations for the elbow. Thus signal J_f excited the elbow flexor and signal J_e excited the elbow extensor channel. This was accomplished by simply adding these inputs to the excitatory parts of equations otherwise identical to equation (14).

The FLETE model equations have been used in prior reports (Bullock and Contreras-Vidal, 1993; Bullock and Grossberg, 1989, 1991, 1992) to explain a number of properties of neuromuscular control, including yielding-compensating properties of the size principle of motoneuron recruitment, the ability to voluntarily vary joint stiffness without inadvertently changing posture, and emergence of multiphasic burst patterns in the EMGs associated with rapid, self-terminated joint rotations.

Adaptive side-loop processing: The cerebello-olivary model

The cerebello-olivary model network is schematized in the upper right part of Figure 2 and in Figure 4. Table 2 contains current anatomical and neurophysiological data on the cerebellum that supports the cerebello-olivary network. Purkinje cell activation obeys:

$$\frac{d}{dt}p_i = 2[-2p_i + (1 - p_i)(25\sum_k g_k z_{ki} + t_i + f(p_i) + .3) - (.8 + p_i)(.1p_j + b_i)], \qquad (32)$$

where z_{ki} is an adaptive weight that multiplies the sampling signal g_k carried by the parallel fibers from the kth granule cell to the ith Purkinje cell, t_i is a climbing fiber teaching signal generated by the ith olivary zone, $f[w] = w^3/(.25 + w^3)$ is a self-excitatory sigmoid signal function, and b_i is stellate/basket cell inhibitory input. Inhibitory stellate/basket-type interneurons were modeled with

$$\frac{d}{dt}b_i = -b_i + 3(2 - b_i)(\sum_k [g_k - 0.4]^+), \qquad (33)$$

where g_k is the activity of the kth granule cell which implies that these cells share parallel fiber receptive fields with the Purkinje cells that they inhibit.

Elements of the NIP/RN stage were modeled with

Connection Type	Citations
mossy fiber $\xrightarrow{+} g_i$, $\xrightarrow{+} n_i$	Shinoda *et al.* (1992)
$t_i \xrightarrow{+} n_i$	Courville *et al.* (1977)
mossy fiber $\xrightarrow{+} l_i$ $g_i \xrightarrow{+} l_i$	Eccles, Ito, & Szentágothai (1967)
$l_i \xrightarrow{-} g_i$	Reviewed in Llinás (1981)
$p_i \xrightarrow{-} n_i$	Ito & Yoshida (1966) Ito *et al.* (1970)
Fractured somatotopy	Eccles *et al.*, (1971a, 1971b) Reviewed in Bloedel and Courville (1981)
t_i electrotonic coupling	Llinás *et al.* (1974) Mano *et al.* (1989)
$t_i \xrightarrow{+} p_i$	reviewed in Bloedel & Courville (1981)
mossy $\xrightarrow{+} g_i \xrightarrow{+} p_i \xrightarrow{-} n_i$ $t_i \xrightarrow{+} p_i$ dendrites mossy $\xrightarrow{+} g_i \xrightarrow{+} b_i \xrightarrow{-} p_i$	Eccles (1977)
LTD and LTP at $g_i \xrightarrow{+} p_i$ synapses	Hirano (1990,1991), Sakurai (1987) Crepel *et al.* (1996)
$n_i \xrightarrow{+} \alpha - MN$	Henatch *et al.* (1986); Robinson *et al.* (1987)
$n_i \xrightarrow{-} $ Renshaw cells	Henatch *et al.* (1986)

Table 3: Evidence for connectivity and physiology incorporated in the cerebello-olivary model

$$\frac{d}{dt}n_i = 2[(-2n_i + (1 - n_i)(0.2 + 2500G[V_i]^+) - (0.8 + n_i)p_i]. \tag{34}$$

Thus the simulated model made no distinction between NIP and RN processing, and assumes that each NIP/RN zone receives only one desired velocity signal. An earlier report (Bullock, Fiala, Grossberg, 1994) showed that such specificity could be learned in NIP because climbing fibers (and the teaching signals that they carry) project both to a limited cortical microzone and to the deep nuclear cells that receive inhibition from that region of cerebellar cortex. Such learning was not modeled in this study, although its outcome was assumed.

The granule cells were modeled with

$$\frac{d}{dt}g_i = 2[-2g_i + (1 - g_i)(.2 + 25,000G[V_i]^+) - (.8 + g_i)l_i], \tag{35}$$

where $G[V_i]^+$ is a desired velocity input assumed to be projected to the granule layer by the mossy fiber pathway, and l_i is Golgi cell input. This equation indicates that granule cells were excited by desired velocity signals and inhibited by Golgi cells. The Golgi cells were modeled as excited by both desired velocity inputs and granule cell outputs:

$$\frac{d}{dt}l_i = -l_i + (2 - l_i)(25,000G[V_i]^+[g_k]^+). \tag{36}$$

This type of granule-Golgi interaction filters the input to produce transient outputs from granule cells with increasing and greater-than-average excitatory input levels. In these simulations, Golgi modulation served to shorten the duration for which the desired velocity input produced granule output and to differentiate the velocity signal to obtain a phase lead.

The adaptive weights z_{ki} from parallel fibers onto Purkinje cells were adjusted up (LTP) and down (LTD) within a range from 0 to 1 according to the learning law:

$$100\frac{d}{dt}z_{ki} = g_k[30(1 - z_{ki}) - 100t_ip_iz_{ki}], \tag{37}$$

where g_k is the parallel fiber signal from the kth granule cell to the ith Purkinje cell. Term t_i is the climbing fiber teaching signal. This equation embodies the hypothesis that LTP occurs whenever parallel fiber synapses are active without coincident climbing fiber activity, whereas LTD requires that both parallel fiber and climbing fiber signals be non-zero (Fiala *et al.*, 1996; Ito, 1991; Ito and Karachot, 1992). In addition, if an antagonist Purkinje cell activity p_j inhibits p_i, as in (32), then learning may not occur in (37) even if t_i and g_k are positive. The learning law (37) hereby realizes a type of opponent learning via the voltage-dependent p_i. If it is empirically the case that the climbing fiber burst invariably depolarizes the Purkinje cell, then a learning law without p_i would be functionally equivalent.

The climbing fiber teaching signal t_i was set equal to the output of the inferior olive network. Each muscle-related channel i of this network, indicated by a site O_i in Figure 2, was composed of two model neurons: an excitatory projection neuron with activity t_i and an inhibitory interneuron with activity u_i (Ellias and Grossberg, 1975). The olivary projection neuron is inhibited by the interneuron and excited by spindle error feedback signals from the associated muscle. The olivary interneuron is excited by, and slowly tracks the activation level of, the projection neuron. This system generates a phasic excitatory burst whenever the excitatory input from the spindle exhibits a significant increase in amplitude. However if the input then remains the same, or decreases, the phasic burst will not be repeated, because of the inhibitory feedback to the projection neuron via the interneuron. Thus:

$$\frac{d}{dt}t_i = -2t_i + (1 - t_i)(33.3[t_i - .4]^+ + E_i) - 33.3t_i[u_i - .4]^+ \tag{38}$$

and

$$\frac{d}{dt}u_i = .1(-u_i + t_i), \tag{39}$$

where the spindle activation E_i is defined by (29). By transforming a step increase into
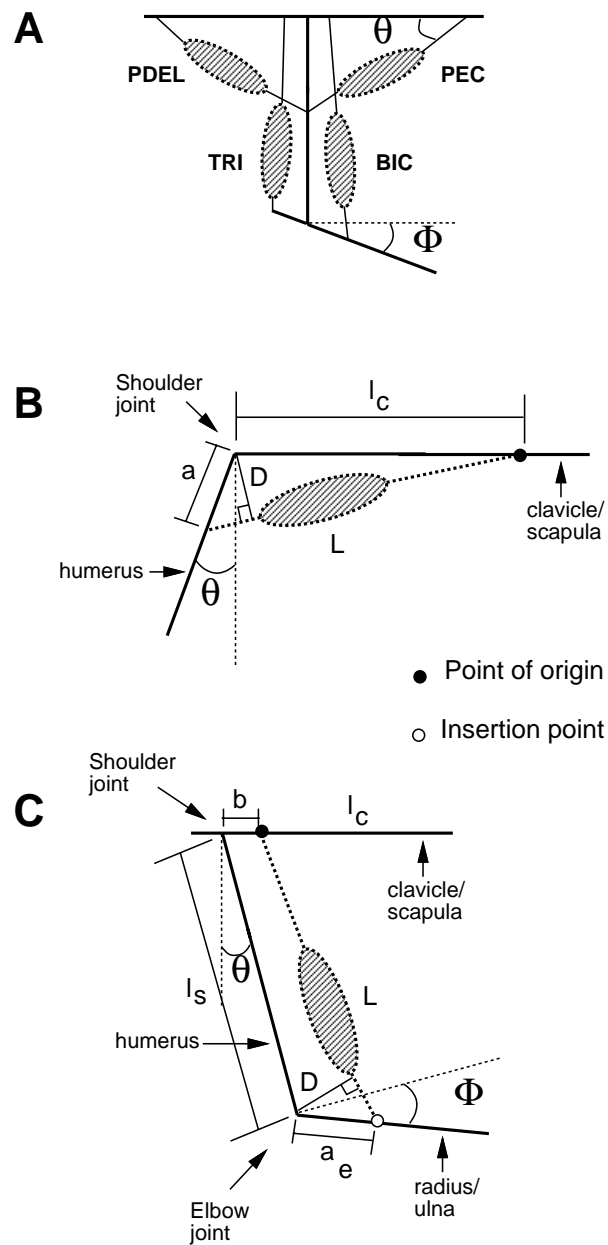
Figure 3: (A) Geometry of origin and insertion points for mono- and bi-articular muscles. Monoarticular muscles (PDEL and PEC) cross one joint, biarticular muscles (BIC, TRI) cross two joints. (B) Schematic of PEC muscle geometry (and that of its antagonist PDEL). (C) Schematic of BIC muscle geometry (and that of its antagonistic TRI). Keys: Θ, shoulder joint angle; Φ, elbow joint angle. a, insertion point for shoulder mono-articular muscle; a_e, insertion point for elbow bi-articular 2 muscle; l_c, distance from clavicle/scapula to shoulder joint; l_s, length of humerus; b, muscle origin distance from shoulder joint; D, normal to the line of pull of muscle.

a pulse, this circuit improves stability by preventing the path through the olive to the NIP from operating as a continuous negative feedback pathway. It also delimits the time during which the teaching signal acts in cerebellar cortex, which is needed for precise adaptive timing. However, use of recurrent feedback from the slow inhibitory interneuron also makes the olive inherently oscillatory. In the present context, this experimentally observed property (Llinás, 1989) is treated as a side effect rather than as a key functional property.

Dynamics formulation of two DOF planar arm

Some simulations of the model incorporate equations (Asada and Slotine, 1986) for a two degree-of-freedom planar arm (Figure 3) that were based on parameters of the human arm. Here we replace (8) as follows. Assuming moment arms constant and equal to 1, the net torque produced by the muscles (pectoralis and posterior deltoid) acting at the shoulder becomes

$$F_{pec} - F_{pd} = \tau_1 = H_{11}\ddot{\Theta} + H_{12}\ddot{\Phi} - h\dot{\Phi}^2 - 2h\dot{\Theta}\dot{\Phi} + G_1 + b_1\dot{\Theta}. \tag{40}$$

The net torque produced by muscles (biceps and triceps) acting at the elbow becomes:

$$F_{bic} - F_{tri} = \tau_2 = H_{22}\ddot{\Phi} + H_{12}\ddot{\Theta} + h\dot{\Theta}^2 + G_2 + b_2\dot{\Phi}, \tag{41}$$

where

$$H_{11} = m_1 l_{c1}^2 + I_1 + m_2[l_1^2 + l_{c2}^2 + 2l_1 l_{c2}cos(\Phi)] + I_2 \tag{42}$$

$$H_{22} = m_2 l_{c2}^2 + I_2 \tag{43}$$

$$H_{12} = m_2 l_1 l_{c2}cos(\Phi) + m_2 l_{c2}^2 + I_2 \tag{44}$$

$$h = m_2 l_1 l_{c2}sin(\Phi) \tag{45}$$

$$G_1 = m_1 l_{c1}g\,cos(\Theta) + m_2 g\,\{l_{c2}cos(\Theta + \Phi) + l_1 cos(\Theta)\} \tag{46}$$

$$G_2 = m_2 l_{c2}g\,cos(\Theta + \Phi), \tag{47}$$

where Θ represents the shoulder joint angle in a planar horizontal arm, Φ represents the elbow joint angle, g represents the acceleration of gravity along the negative y axis, and b_1 and b_2 are viscosity coefficients that account for friction at each joint. Though viscosity may be a function of position, velocity, and joint stiffness, in this study it is assumed to be constant. The product of viscosity and angular velocity is important in achieving stability of the limb. We used typical estimates of segment masses (m_i) and segment lengths (l_i) and inertial characteristics from anthropometric data (see Table 4) of Zatsirosky and Seluyanov (1983) and Karst and Hasan (1991).

In our simulations, the shoulder and the elbow are restricted to one rotational degree of freedom (flexion-extension). The muscles whose actions are modeled in these simulations are listed in Table 5 and depicted in Figure 3: Posterior Deltoid (PDEL), Pectoralis Major (PEC), Biceps (BIC), and Triceps (TRI). To compute muscle lengths, we assumed rotary joints affected by two opponent muscles (i.e., agonist and antagonist), each of which is

Parameter	Value
m_1	$1.97\ kg$
I_1	$1.3\ \times\ 10^{-2}\ kg\ m^2$
$l_1 = l_s$	$36.0\ cm$
m_2	$1.64\ kg$
I_2	$2.7\ \times\ 10^{-2}\ kg\ m^2$
l_2	$47.0\ cm$
$l_{c1} = l_1/2$	$18.0\ cm$
$l_{c2} = l_2/2$	$23.5\ cm$
$b_1,\ b_2$	$.3\ Nm.s/rad$
$l_c = l_1/2$	$18.0\ cm$
b	$1\ cm$

Table 4: Anthropometric parameter values for the upper limb.

Muscle	Origin	Insertion	Type
Biceps-long head, BIC	glenoid fossa	radius	biarticular
Triceps-lateral head, TRI	fossa of scapula	ulna	biarticular
Pectoralis major, PEC	clavicule	humerus	monoarticular
Deltoid-posterior, PDEL	scapula	humerus	monoarticular

Table 5: Upper arm muscles.

inserted in the moving segment distal to the axis of rotation. The distance from muscle origin to the axis of rotation was given by l_j, $j = c$, s, (see Table 1) and the midpoint of the joint's 180° excursion was stipulated to be at joint angle $\Theta = 0^o$ and $\Phi = 0^o$ for the shoulder and elbow, respectively. Origin-to-insertion muscle lengths are a function of angle Θ for the single-joint muscles, but are functions of Θ and Φ for bi-articular muscles. It is assumed that the distance, $l_{ci}, i = 1, 2$, to the center of mass of each segment link equals half of the length of the line joining the two ends of the link.

The PEC and PDEL muscles are single-joint muscles, and their length at a given rotation can be computed as follows:

$$L_{pd} = \sqrt{(l_c + a\ sin(\Theta))^2 + a^2\ cos^2(\Theta)} \tag{48}$$

where L_{pd} is the length of the PDEL muscle, l_1 is the distance from the clavicle/scapula to the shoulder joint, $a = 10$ cm. is the insertion distance from the proximal (shoulder) joint, and Θ is the angle of rotation centered at $\Theta = 0^o$ (see Figure 3). For the PEC muscle,

$$L_{pec} = \sqrt{(l_c - a\ sin(\Theta))^2 + a^2\ cos^2(\Theta)} \tag{49}$$

Moment-arms were assumed to be constant over the whole range of limb movements and

their values were fixed at 1.0. Alexander (1981) has noted that the angle of pennation – namely, the angle at which the muscle fibers pull with maximum force – is approximately a constant between 0.87-1.0, which is why the moment arm can be considered constant. In the case of the BIC and TRI, the muscles cross two joints; therefore, the shortening of these muscles is affected by both the elbow joint angle and the shoulder joint angle. We can approximate the length of these muscles as follows (see Figure 3). In the case of TRI,

$$L_t = \sqrt{(l_s + a_e \ sin(\Phi) - b \ sin(\Theta))^2 + (a_e - b)^2 cos^2(\Phi)} \tag{50}$$

where $a_e = 15$ cm. is the muscle insertion distance from the elbow joint, $b = 1$ cm. is the muscle origin distance from the shoulder joint, l_2 is the humerus length, Θ is the angle of rotation of the humerus segment with respect to the vertical, and Φ is the rotation angle of the forearm with respect to the humerus. In the case of the BIC muscle,

$$L_b = \sqrt{(l_s - a_e \ sin(\Phi) - b \ sin(\Theta))^2 + (a_e - b)^2 cos^2(\Phi)} \tag{51}$$

Note that the lengths of BIC and TRI can not be related simply to angle Φ of the elbow joint. The muscle lengths for biarticulated muscles depend on both the elbow angle and the shoulder angle.

3   Results

In this section we present three sets of results. First, we show how adaptive weights evolve in cerebellar cortex when the simulated limb is exercised by a long series of attempted movements. We show that weight evolution converged and was such as to establish a reciprocal pattern of function at this level of the system. Thus the learning rule is both stable and capable of pruning an initial connectivity to increase efficiency. Second, we show that model NIP/RN activity after learning exhibits phasic bursting, with burst amplitude a function of desired movement rate. This result corresponds to observations of cells in the NIP and the magnocellular portion of the RN, which gives rise to the rubro-spinal projection (e.g., Gibson *et al.*, 1985; Martin and Ghez, 1991). We also show that both aspects of the dual projection from RN to the spinal cord are important. In particular, the inhibition of Renshaw cells transiently enhances the gain of the stretch reflex (Henatsch *et al.*, 1986; Hultborn, Lindstrum, and Wigstrom, 1979) and prevents premature truncation of alpha MN bursts needed to launch and brake rapid movements. Third, we show that the model learns to substantially improve the execution of a two-joint movement by compensating for mechanical interactions between the two moving segments. Because this improvement is measured relative to a decerebellate version of the model, which lacked both the model cerebellum and its output to spinal circuits via the rubro-spinal pathway, the improvement is directly attributable to the adaptive cerebello-rubro-spinal system.

Learning and emergence of reciprocal patterning in cerebellar cortex

A major feature of the cerebellar cortex is the asymmetry between the impressive fan out of signals carried by mossy and parallel fibers to widely distributed Purkinje cells and the restricted distribution of signals carried by climbing fibers to bounded sets of Purkinje
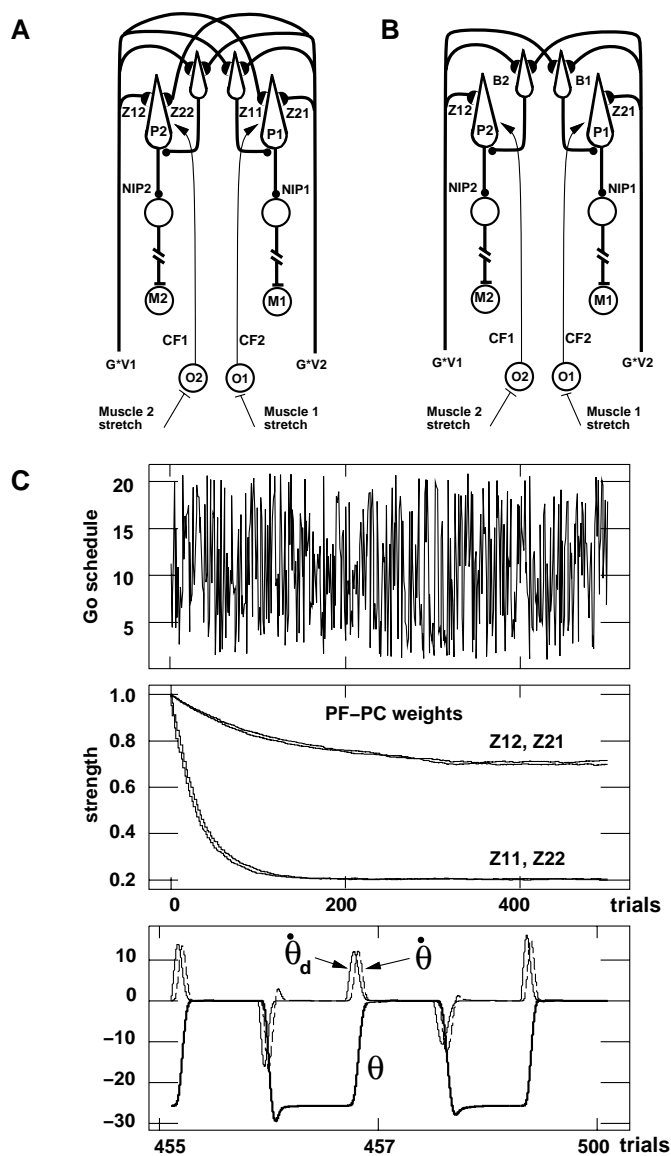
Figure 4: Opponent cerebellar connectivity before (A) and after (B) learning. All the synaptic weights between parallel fibers and Purkinje cells were initially set to 1. During learning, weights in signal pathways Z_{22} and Z_{11} shown in (A) are diminished through parallel fiber to climbing fiber long-term depression resulting in the connectivity shown in (B). (C) Model simulations with cerebellar feedforward learning. (Top) Random gain schedule for the GO signal multiplier during arm movement involving cyclic 25 degree flexion and extension; the GO schedule was randomized over 500 trials (uniform distribution between 1 and 20) to vary the movement speed. (Middle) Learning at parallel fiber-Purkinje cell synapses is stable and approaches a steady state after about 400 movement trials; (Bottom) Joint position (Θ) and velocity ($\dot{\Theta}$) traces during the last five movement trials. The joint velocity $\dot{\Theta}$ trace shows that the system is able to dynamically track the desired joint velocity $\dot{\Theta}_d$.

cells within parasagittal microzones (Ito, 1984). This is mimicked in the model by the distribution of desired velocity signals, via the mossy-granule-parallel fiber pathway, to all Purkinje cells in the model, combined with distribution of each climbing fiber to only one Purkinje cell associated with a single NIP/RN zone and its target muscle; namely, that muscle whose stretch receptors project to the olivary zone giving rise to that climbing fiber.

A first question to ask is whether the restricted CF distribution leads to selective disinhibition of only that NIP/RN site which also receives the desired velocity input and whose projection to spinal cord can help activate the muscle whose contraction is desired. Figure 4 schematizes the network before (panel A) and after (panel B) the learning that occurred during a series of single joint flexions and extensions performed by the three component model. Figure 4C shows that the weight change is initially fast, but becomes asymptotic over this series of learning trials. After learning, the parallel fiber projection of the velocity signal $G[V_1]^+$ command in (35) to p_1 in (32) has been functionally deleted from the network by LTD, but the projection to p_2 remains. As a result, $G[V_1]^+$ onset acts at the NIP stage to excite n_1 and in the cerebellar cortex to inhibit p_1. The latter effect is achieved because $G[V_1]^+$ excitation of p_1 has been removed whereas the parallel fiber projection of $G[V_1]^+$ continues to excite two sources of inhibition to p_1, namely b_1 in (33) and p_2 in (32). Such unopposed inhibition of p_1 leads it to pause, which opens the gate for passage of part of the $G[V_1]^+$ command through the NIP stage. A recent report on adaptive timing in cerebellum (Fiala *et al.*, 1996) proposed an additional source of Purkinje cell pausing that may complement those simulated here.
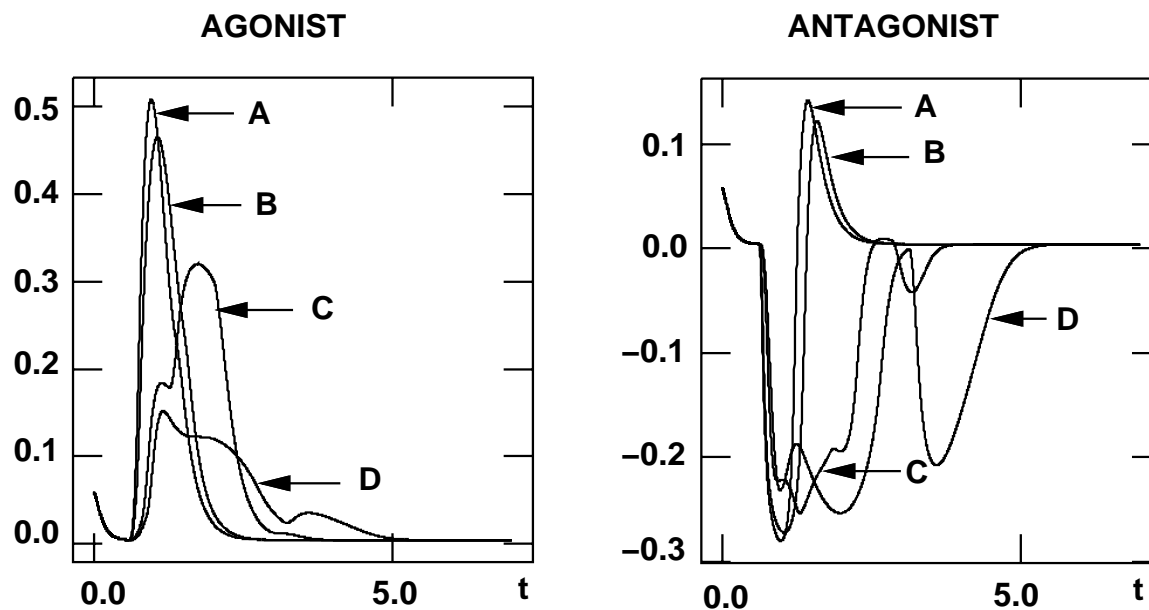
Figure 5: Parametric analysis of the NIP response to movement of different speeds. (LEFT) Response of the agonist NIP cell; and (RIGHT) antagonist NIP pool. Condition A corresponds to the faster movement, and condition D corresponds to the slower movement. Two intermediate conditions (B) and (C) are also presented. The input were the desired velocity vector $(G[V]^+)$ signal from the VITE circuit.

(A) DECEREBELLATE
Joint variables

(B) INTACT
Joint variables

(C) RENSHAW LESION
Joint variables

(D) α-MN LESION
Joint variables
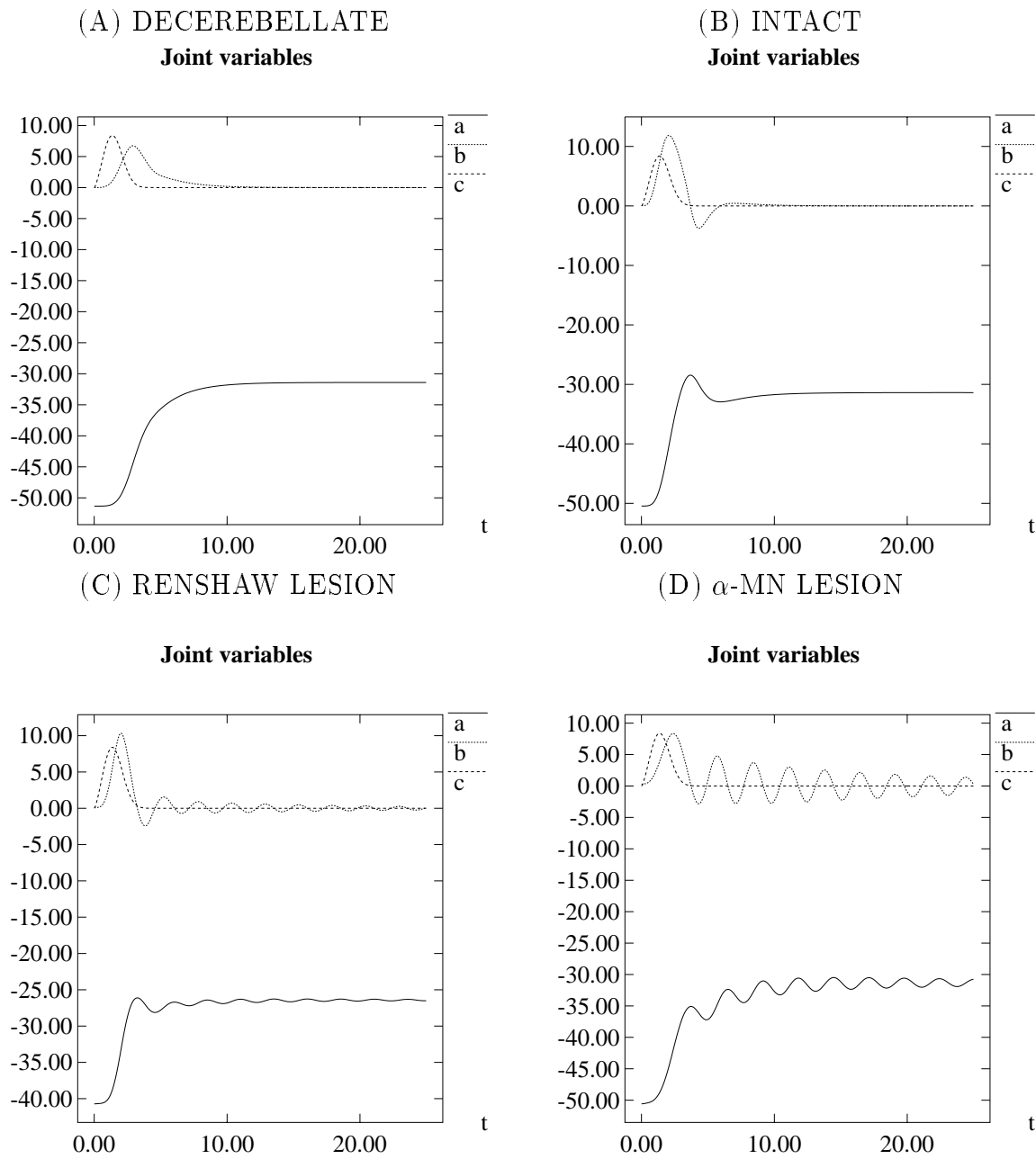
Figure 6: VITE-FLETE-CEREBELLUM model simulations for (A) decerebellate network, (B) intact system, (C) missing inhibitory projections from NIP/RN to Renshaw cells and (D) missing excitatory projections from NIP/RN to α-MN. Keys: trace a represents the joint trajectory, b represents the joint velocity, and c represents the desired velocity command.

Biphasic burst activity of deep nuclear cells and effects of the dual projection from RN to spinal circuits

An important benchmark for a cerebellar model is data collected in recent decades on phasic activities of cells in the NIP and in its primary projection target, the magnocellular zone of the RN. In many studies, phasic activity increments in RN have appeared only in cells associated with the agonist muscle (Gibson, *et al.*, 1985; Martin and Ghez, 1991) and the extended durations of these bursts have led some to interpret the RN signal as a velocity command. In our simulations as well, shown in Figure 5, medium and low speed movements produced agonist channel bursts whose duration was similar to that of the entire movement, hence might be interpreted as velocity commands (if one were to ignore the actual structure of the model). However, when the speed of desired movement was increased, the agonist channel burst at the NIP/RN was significantly shortened, and there emerged a following burst in the antagonist channel of the NIP/RN. This bursting pattern was more reminiscent of the multi-phasic burst pattern that is observed at the level of the EMG during rapid joint rotations, in which a large braking burst in the antagonist becomes necessary to prevent limb inertia from causing a large overshoot relative to the intended endpoint of the movement (Lestienne, 1979).

The emergence of a braking burst in the model RN is not surprising since the role of the cerebellum in the current model is to help generate the torques needed to achieve the desired velocity and position. That is, its role is to compute solutions to inverse dynamics problems. The model thus predicts that if RN activity is examined appropriately during rapid practiced movements, the uniphasic pattern reported in many prior experiments should be replaced with a bi-phasic pattern distributed across two subpopulations.

The model also clarifies the functional significance of the dual projection from RN to the spinal circuits. In earlier work, it was proposed (Akazawa and Kato, 1990; Bullock and Grossberg, 1989) that one role of the Renshaw cells is to make the response of the alpha MN pool to excitatory inputs more linear. In the case of an excitatory co-contractive signal sent to both opponent alpha MN pools, such a linearizing effect helps ensure independent control of joint angle and joint stiffness. Such independence is quite important in postural control, when an animal may want to stiffen a joint without changing the difference between the forces acting across the joint.

Movement, however, often requires rapid sequencing through large differences in the forces acting across the joint. Rapid rises of force toward the maximal voluntary force level are impossible unless Renshaw inhibition is curtailed during the rise time. Because one leg of the dual descending projection from the RN inhibits Renshaw cells, the cerebellum is capable of transiently shifting the alpha MN pools out of the near-linear regime created by Renshaw feedback and into the nonlinear regime made possible by the size principle of alpha MN recruitment. Figure 6 depicts the tracking capabilities of four networks corresponding to the entire circuit of Figure 2 or various subsets thereof. In all cases, the same desired trajectory was generated, for a flexion movement that started from an initially extended joint position. The desired velocity profile appears in each panel as dotted trace c, whereas the realized velocity appears as trace a and realized position as trace b. Figure 6A shows the decerebellate case, where the dynamics of the movement are poor compared to the ideal velocity profile. The movement develops slowly and the reaction time is prolonged as seen from the difference between the onsets of desired and actual joint velocities. The

joint velocity has a long right tail, and the rise time is slow.

When only the RN projections to Renshaw cells are eliminated (Figure 6C), the system shows end-point oscillations that are abnormally prolonged. Cutting the NIP/RN projection to the Renshaw cells removed input related to the phasic and the tonic baseline components of NIP/RN discharge. A side effect is that the equilibrium values of the system are modified, because the Renshaw cells do not receive the inhibitory tonic baseline activity from the NIP/RN cells. When only the RN projections to the alpha MN pools are eliminated from the system (Figure 6D), the joint initially undershoots the equilibrium position and oscillates around the end-point. This persistent tremor is similar to that seen in cerebellar patients. Without RN inhibition of Renshaw cells, the alpha MN burst and consequent force development are truncated prior to reaching the levels needed for the desired movement rate.

The effects of specific simulated lesions in the NIP/RN projections to the spinal circuit, corresponding to the lower panels of Figure 6, were analyzed in terms of alpha-MN activity and spindle feedback for the network without a NIP/RN to Renshaw projection (Figures 8A, B) and the network without a NIP/RN to alpha-MN pool projection (Figures 8C, D). Both alpha-MN activity and spindle feedback reflect the oscillatory behavior caused by the cerebellar lesions. Figure 8A shows that the agonist burst is stronger than the antagonist, but there is coactivation of both muscles. A comparison of Figures 8B and 7D indicates that this coactivation results in part from an abnormally large collapse of agonist spindle feedback, which releases the antagonist alpha-MN pool from IaIN-mediated inhibition. The collapse of the agonist spindle feedback is in turn due to strong agonist Renshaw inhibition of the agonist gamma MN pool. Thus, the NIP/RN to Renshaw projection normally prevents Renshaw cells from inhibiting gamma MNs and thereby disrupting the IaIN mediated pattern of reciprocal activation of agonists and antagonists. Another source of coactivation is the agonist Renshaw inhibition of the antagonist Renshaw pool, which disinhibits the antagonist MN pool.

Figure 8C shows that the simulated lesion of the NIP/RN to alpha-MN projection led to an abnormally small alpha-MN launching burst (compare with Figure 7C) and to much less coactivation than in the case of the NIP/RN to Renshaw lesion. In fact the delayed antagonist braking burst is nearly normal. This is because the surviving NIP/RN to Renshaw projection disinhibits the antagonist MN pool at the time when the antagonist spindle feedback signal is growing and the IaIn mediated inhibition is at a minimum because of collapse of agonist spindle activity. Thus there is a large transient enhancement of the gain of the antagonist stretch reflex. These effects combine to produce the initial undershoot observed in Figure 6D.

Equilibria of the 2D planar arm

To illustrate the cerebellar opponent learning capabilities using a 2D planar arm with mono- and bi-articular muscles, we used two independent single-joint VITE-FLETE systems (Bullock, Contreras-Vidal, and Grossberg, 1993a; 1993b). Each FLETE system generates the muscle forces needed to move its corresponding arm segment (e.g., shoulder or elbow joint) by contracting the appropriate muscles according to the planned movement. The biomechanics of the 2D planar arm included the full dynamic equations described earlier (Equations (40) and (41)), except that the gravitational effects were neglected by
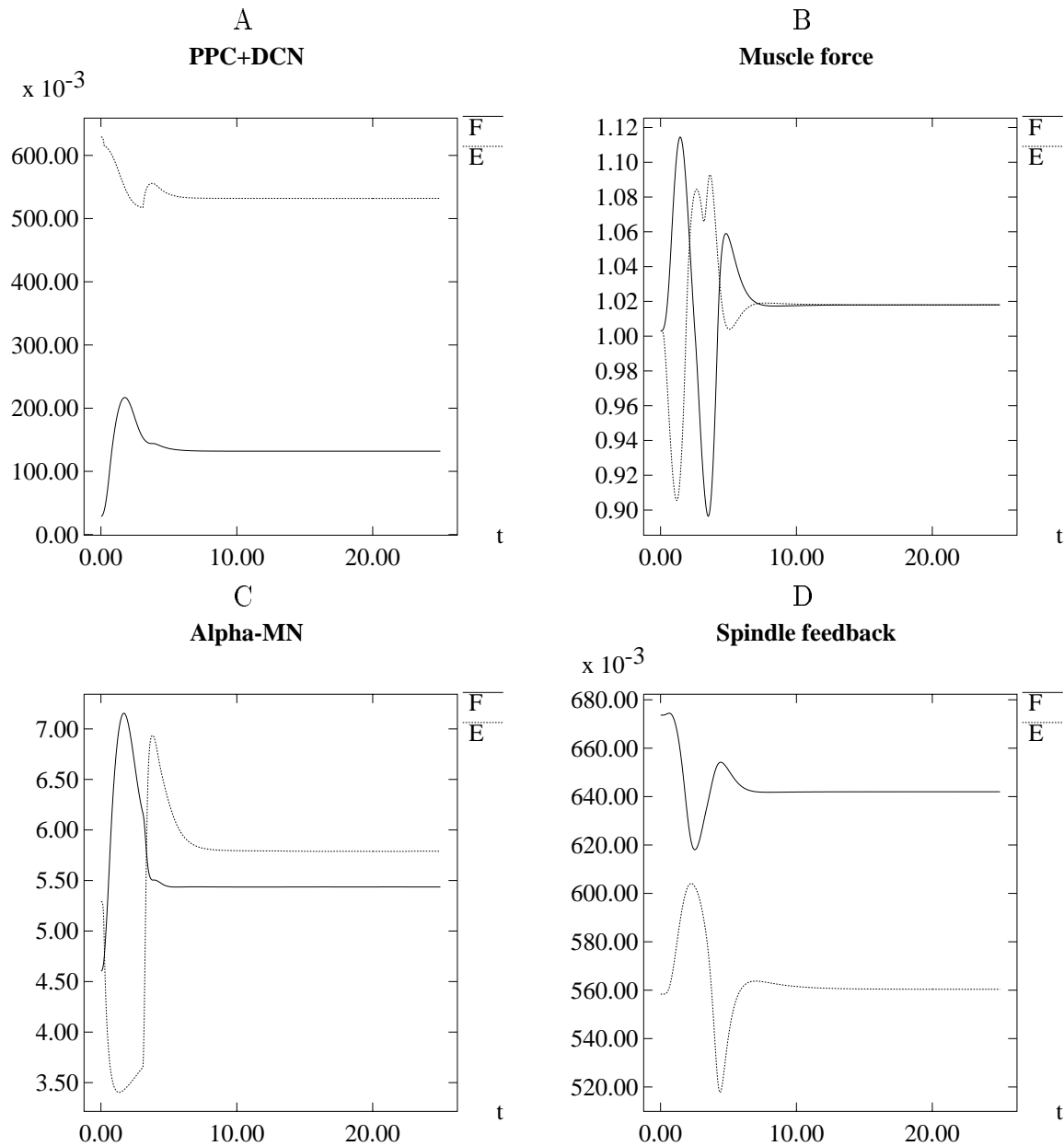
Figure 7: This figure depicts key variables from flexor and extensor channels for the intact network simulation of Figure 6. Figure 7A shows the net input to the alpha-MN pools. This input is composed of phasic, burst-like NIP/RN output signals superimposed on ramp-like opponent outputs from the PPV stage of the CPG. The simulated EMG activity in Figure 7C shows a bi-phasic patterning of muscle activity (AG followed by an ANT burst), while the simulated muscle forces in Figure 7B represent a tri-phasic pattern (large AG, ANT, small second AG). The reciprocal spindle feedback activities are shown in Figure 7D.
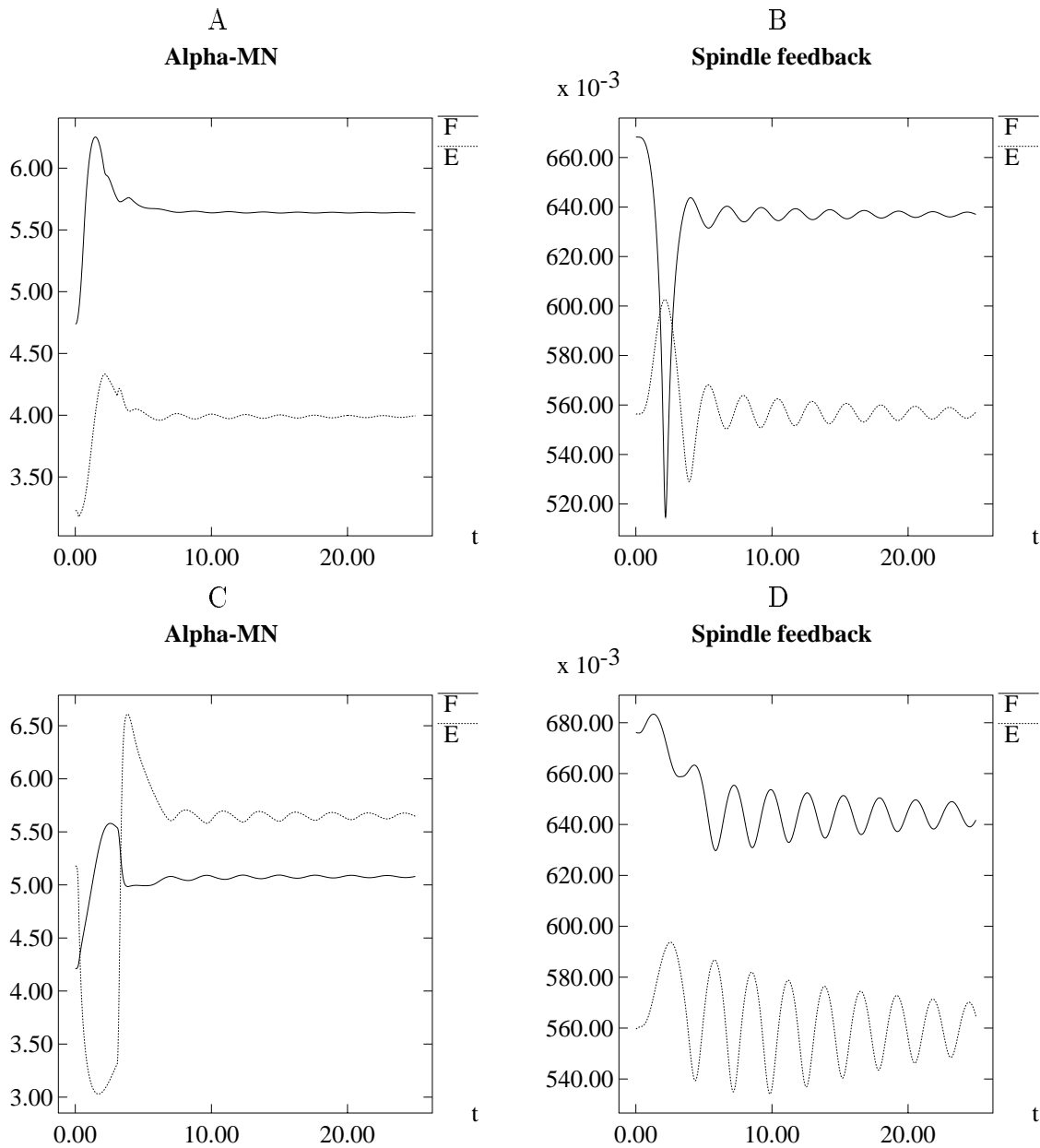
Figure 8: VITE-FLETE-CEREBELLUM model simulations showing α-MN activity and spindle feedback when the projection from NIP/RN to Renshaw cells is eliminated (A & B), and when the NIP/RN to α-MN projection is damaged (C & D), in the simulations of Figure 6. Both simulated lesions produce end-point oscillations, but the latter lesion is more damaging.

assuming a pure horizontal movement; i.e., $g = 0$ in (46) and (47). Figure 9 depicts the steady-state response of the planar limb controlled by a decerebellate multijoint VITE-FLETE system. Joint angles for the shoulder and elbow as a function of the difference between the descending PPV commands, that is $A_1 - A_2$ (see Figure 2 and equations (9) and (10)), are shown for each joint.

In the absence of external loads, the difference $A_1 - A_2$ would specify a unique equilibrium joint angle in a one-joint FLETE system. Because we here have a coupled system, each set of plots represents joint angle for a given joint (e.g., shoulder or elbow) versus $A_1 - A_2$ while the other joint received constant input. Positive values of $A_1 - A_2$ mean joint flexion, and negative values mean joint extension. Simulations are shown for a system with and without joint afferent feedback from the shoulder joint to the elbow motoneurons. Panel A depicts the steady state behavior of the shoulder joint angle to the difference $A_1 - A_2$ when the elbow joint received constant input ($A_1 - A_2 = 0.08$). The simulation shows that the shoulder angle is approximately a linear function of the difference $A_1 - A_2$, but the elbow angle rotates (in the extension direction) as the shoulder moves across the workspace. The rotation of the elbow joint is increased for higher coactivation values (e.g., the effect is greater for a co-contraction value, in (9) and (10) of $P = 0.4$ than for $P = 0.3$). This is understandable because the elbow muscles are bi-articular muscles and depend on the shoulder angle. Furthermore, during shoulder flexion, the BIC muscle is unloaded and an imbalance is produced in favor of the antagonist TRI muscle resulting in the elbow extension. Thus, there was a partial breakdown of the basic FLETE property that the joint angle associated with any choice of $A_1 - A_2$ remains invariant across changes of joint stiffness due to varying the coactivation signal P in (9), (10), (14), (16), (22), and (25). To compensate, feedback signals (30) and (31) from the shoulder joint receptors act on the elbow motoneuron pools. Joint receptors respond to increased flexion of the shoulder joint by projecting to the flexor α-MN pool for the elbow, therefore increasing elbow flexion. Because this feedback is position-dependent and monotonic, the outcome is elbow stabilization. This is shown in Panel A of Figure 9. In particular, the addition of joint receptor feedback allows the elbow angle to remain constant for a given choice of $A_1 - A_2$ over the full range of shoulder angles. Panel B illustrates that the compensation suffices across the workspace.

Performance of cerebellate and decerebellate versions of the model in the control of a two-joint arm movement

This section shows how cerebellar learning in an opponent motor controller can adaptively discover and form muscle synergies in the case of multi-joint arm movements. For a two-joint arm moved by both mono- and bi-articular muscles, the feedback learning process can be summarized as shown in Figure 10. Planar reaching produced by the interplay of two pairs of agonist muscles admits four cases as tabulated in Figure 10A. Let us assume that the stretch signals generated during two-joint arm movements in the horizontal plane follow a non-overlapping (alternating, albeit with some degree of coactivation), discrete AG-ANT pattern as shown in Figure 10A. Panel B shows a representation of the network system before learning, Panel C during learning, and Panel D after learning. The rows of panel B correspond to distinct parallel fibers, carrying error information for each muscle channel. Each parallel fiber projects nonspecifically to all the Purkinje cells (P1 through
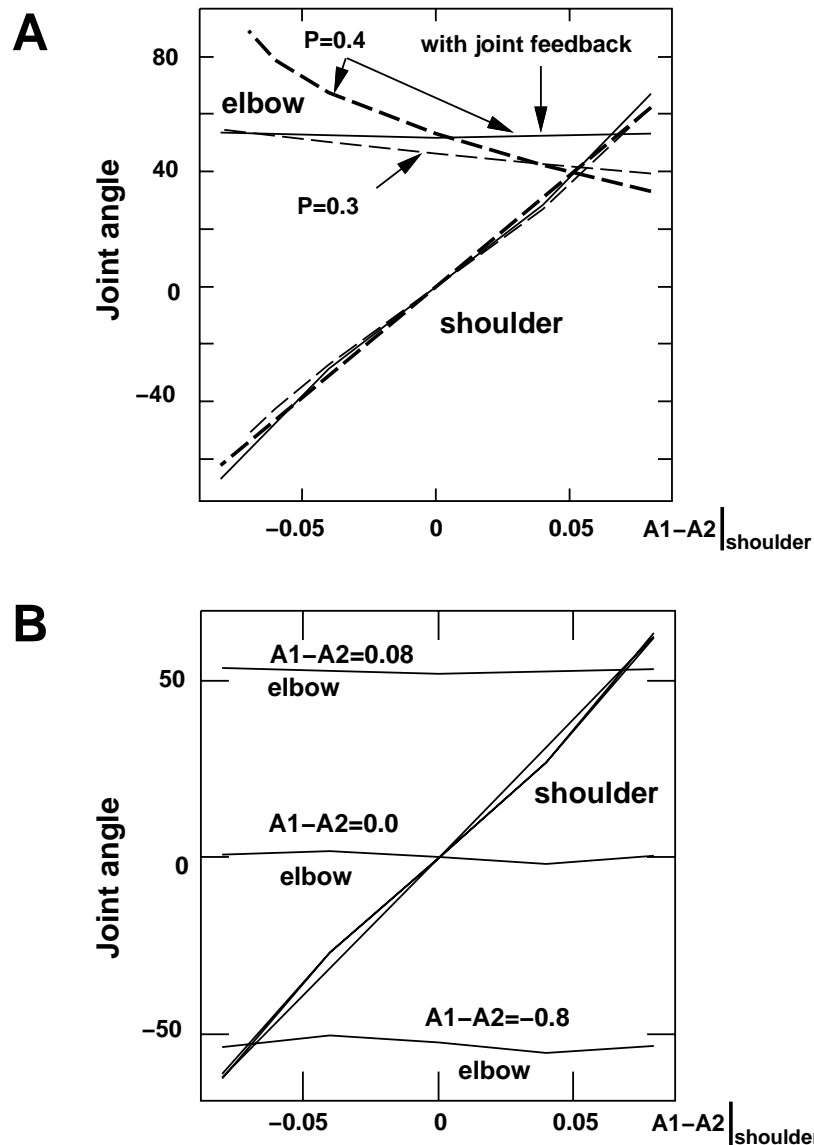
Figure 9: (A) Steady state response of the planar two joint limb with and without feedback joint compensation. Without joint feedback, at coactivation settings of either P=.4 or P=.3, elbow angle changes as shoulder angle changes despite constant settings of desired elbow angle commands. Joint receptor feedback from shoulder joint to elbow joint allows elbow joint angle to remain constant over the full range of shoulder angles if the descending position command for elbow is held constant. This simulation with hypothesized joint receptor feedback used a coactivation value in Equation 9 of P=0.4. (B) The linearity is preserved across the work space. In these simulations, the input to the FLETE elbow system was constant during three different input settings corresponding to three regions covering the workspace of the planar arm ($A_1 - A_2 = .08$, 0, and $-.08$). The input to the FLETE system controlling the shoulder joint was varied from -0.08 to 0.08.

(A)

Case	Shoulder	Elbow	PEC	PDEL	BIC	TRI
1	Flex	Flex	AG		AG	
2	Ext	Ext		AG		AG
3	Flex	Ext	AG			AG
4	Ext	Flex		AG	AG	

(B)

(C)

case 1 case 2 case 3 case 4

(D)
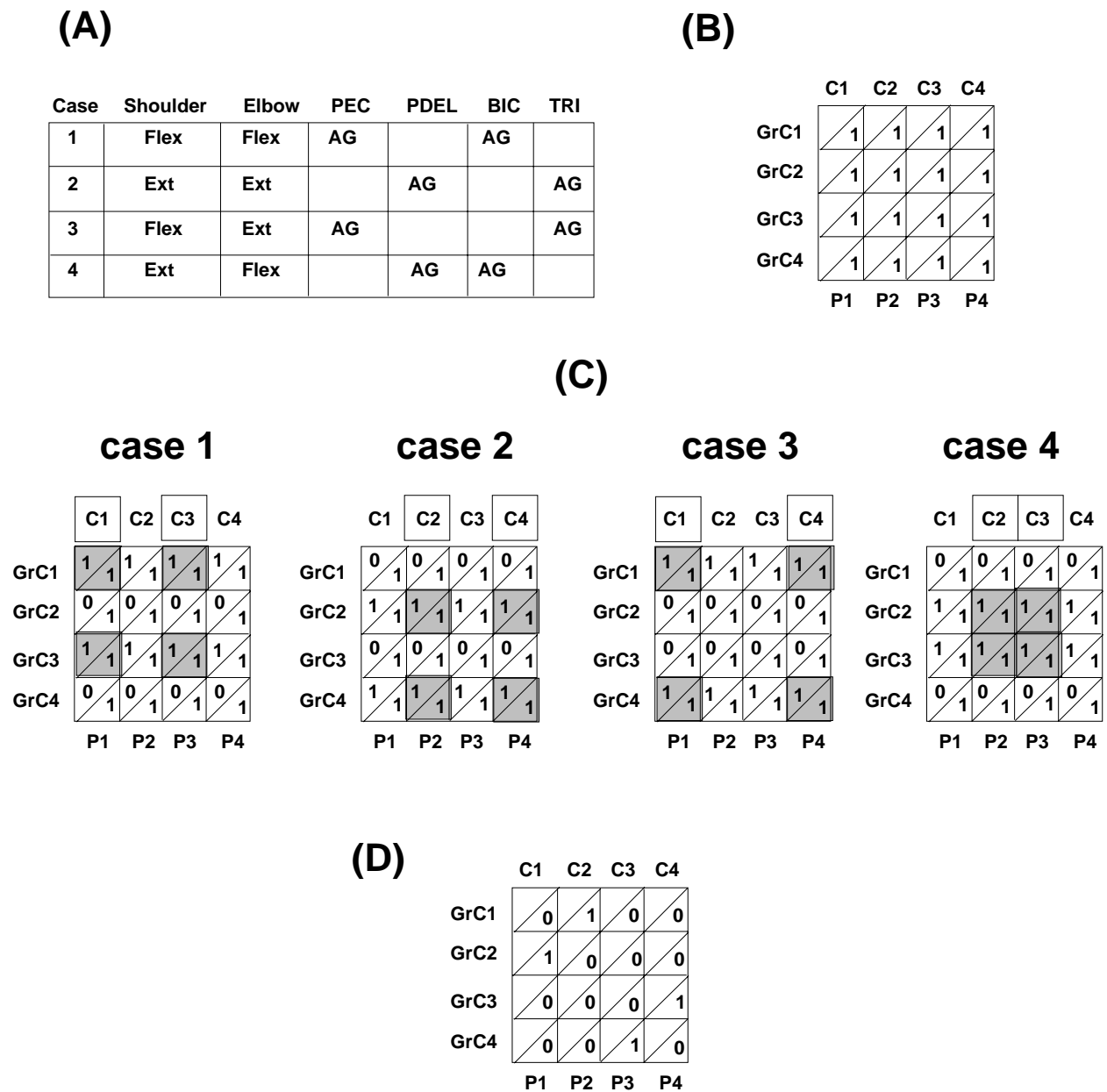
Figure 10: Map representation of the cerebellar connectivity before, and after learning. (A) Four possible cases depicting alternating pattern of EMG activation during planar, horizontal, pointing movements; (B) Before learning, all the synaptic $PF \rightarrow Purkinje$ connections are strong (e.g., set equal to one); (C) LTD-based cerebellar learning; (D) Synaptic matrix after learning.

P4) and cerebellar interneurons (not shown). Initially, the strength of the parallel fiber to Purkinje cell connections are set to one (Panel B). Activity in parallel fibers and climbing fibers are represented by a box enclosing the activated cells. Each column representing a given Purkinje cell may receive specific activation from its climbing fiber (C1 through C4). A co-occurrence of parallel fiber and climbing fiber activation is indicated in Panel C by shading the matrix cell corresponding to the Purkinje axo-dendritic zone where these two signals could converge. In summary, each Purkinje cell can receive parallel fiber inputs from all granule cells, and climbing fiber inputs only from the unique inferior olive afferent innervating it.

Panel C shows the pattern of activations elicited by conjunctive stimulation of parallel and climbing fiber signals for each case shown in Panel A. In case 1, parallel fiber (PF) signals from PF_{1j} and PF_{3j} arrive at all Purkinje cells as shown by the boxes enclosing them. Climbing fiber discharges signaling motor errors in channels C1 and C3 also arrive in close temporal and spatial relationship with those parallel fiber signals. This would produce LTD of the synapses PF_{1j} to $P1$, PF_{3j} to $P1$, PF_{1j} to $P3$, and PF_{3j} to $P3$. After enough trials, encompassing all combinations in panel A, the resulting pattern of connectivity will be like that shown in Panel D. In particular, only the weight from the PF projecting to the opponent PC of the same joint will survive LTD. The resulting connectivity matrix shown in Panel D can produce the following two outcomes: a) a single joint stretch (e.g., due to a external load) elicits reciprocal counteraction in the segment of origin as well as stiffening of the adjacent segment; and b) a two-joint stretch elicits two-joint counteraction.

State space trajectory
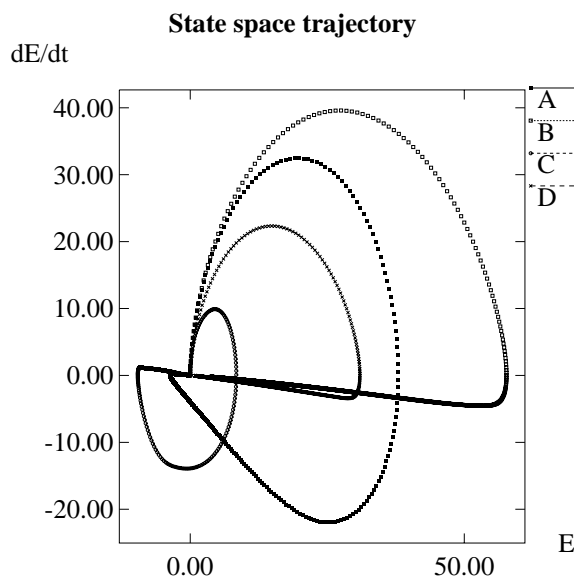
Figure 11: State–space representation of the shoulder and elbow position and velocity tracking for both intact and decerebellate two-joint model simulations. Three variables are shown: The plots show curves of joint position error (x-axis) vs. error derivative (y-axis) for both shoulder and elbow joints over time. Key: $E = \Theta - \Theta_d$ (shoulder) or $E = \Phi - \Phi_d$ (elbow). Plots A (shoulder) and C (elbow) are for the intact system; plots B (shoulder) and D (elbow) correspond to the decerebellate system.

Using the connectivity matrix in Figure 10D we were able to study the performance of the tripartite model of Figure 2 with and without the cerebellar component during a rapid two-joint movement. Figure 11 shows the state space trajectories of elbow and shoulder joints during two movements made with identical CPG settings. One movement was made with the cerebellar component (after learning trials with the two-joint system) and one without. The coordinates for the plotted trajectories are error coordinates: the x-axis is joint position error and the y-axis is joint velocity error, with error measured relative to the desired trajectory generated by the CPG. A perfect performance would be represented by a point at the origin, indicating zero velocity and zero position error throughout the trajectory. That neither system approached perfect performance of the desired trajectory, indicates that the model is not an optimal controller in its present form. This is not surprising because of the restricted state information available to the cerebellum in these simulations and because of our omission of the spectral timing component of cerebellar learning (Fiala *et al.*, 1996). However, what is more important in the present context is that for each joint the excursion away from the origin was much larger for the decerebellate model than for the model with intact cerebellum. This is a graphic illustration of the error-reductive competence of the simulated cerebellar embedding.

Figure 12 shows the simulated kinematics and EMG activities of the 2 joint system with and without cerebellar compensation corresponding to the state space trajectories shown in Figure 11. The decerebellate system was simulated by eliminating the DV*G commands to the cerebellar circuitry, but maintaining the tonic excitation to both Purkinje and NIP cells, so that the tonic influence of the NIP/RN cells upon spinal cord circuitry was intact, and only the phasic component was disrupted. The movement comprised a 65 degrees shoulder extension and a 34 degree elbow extension. For this simulation, all the circuitry from Figure 2 was replicated to control two sets of opponent muscles, one mono-particular (P DEL, PEC), the other bi-articular (TRI, BIC). Biomechanical equations were also modified appropriately, as noted above. Heteronymous joint receptor feedback, from the shoulder to elbow motoneurons, was also added to help compensate for static shoulder joint effects at the elbow. The decerebellate simulation shows smaller amplitude muscle activations and more sluggish limb response than in the intact system.

In Figures 6 through 8, it was shown through simulations of the one joint case that interpositus lesions degraded the ability of the neuromuscular control system to track the desired velocity of the movement, resulting in increased onset latency, rise time and settling time. In this section, we illustrate through simulations the effect of damage to the cerebellar cortex in the 2D system.

Figure 13 shows the effect of a cerebellar lesion on the performance of a multi-joint limb flexion. This simulation was performed by removing Purkinje cell inhibition from the NIP model cells shown in Figures 1 and 2. The effect of this simulated lesion was to take out the cerebellar processing except the direct projections (collaterals) from mossy fibers to NIP cells. This implies that the NIP cells would be disinhibited because of the removal of tonic and phasic Purkinje cell inhibition. In these simulations, it was assumed that the matrix of cerebellar connectivity was already learned (see Figure 10D); in addition, climbing fibers were not sent to the interpositus neurons. Therefore, these simulations address the role of the mossy fiber projection to the NIP cells alone.
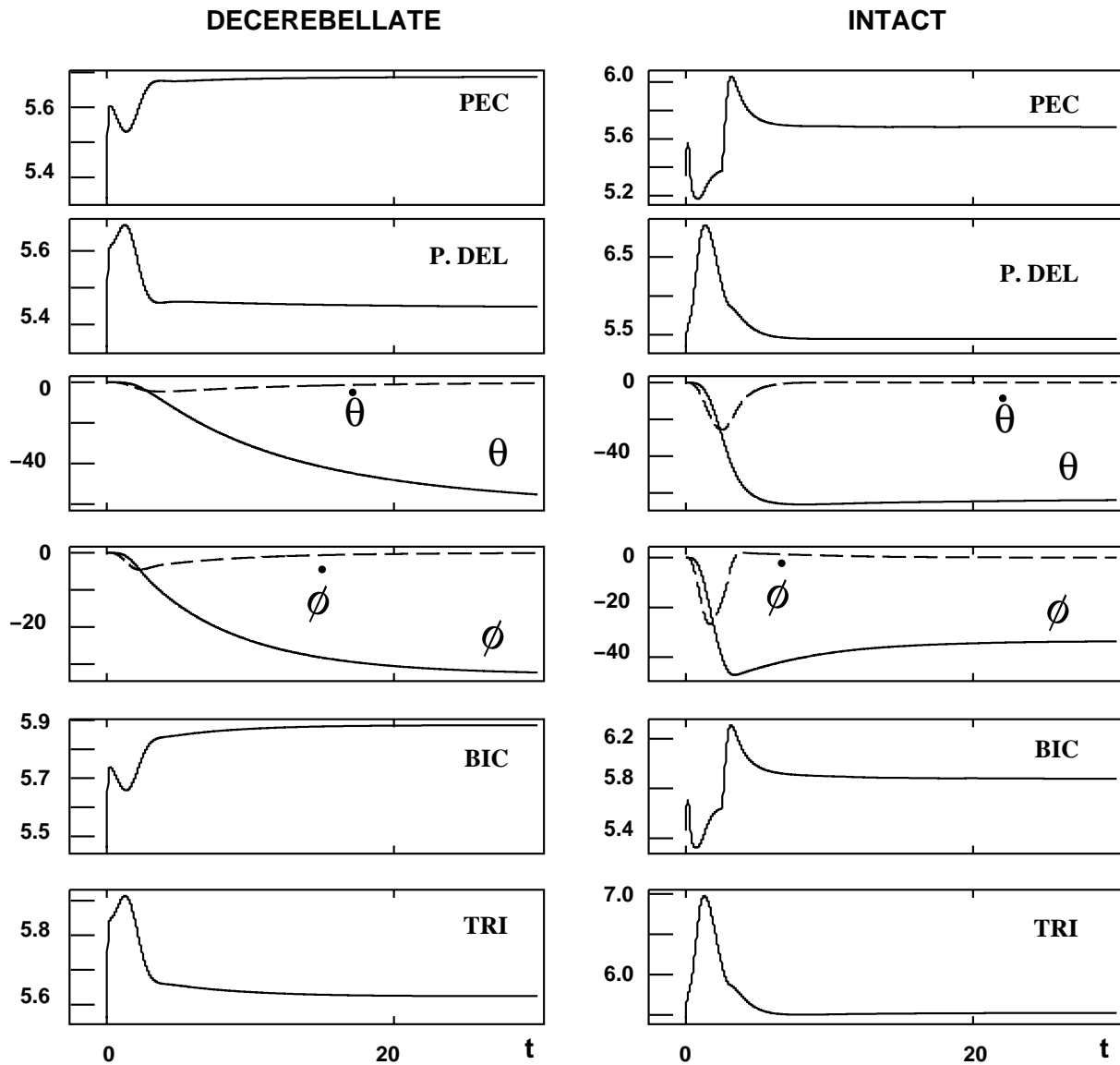
Figure 12: Simulations of the 2-D planar arm using two VITE-FLETE-CEREBELLUM model systems coupled through joint receptors and the bio-mechanics of the arm. Rows 1, 2, 5, and 6 show dynamics of motoneuron activations associated with 4 muscles. Rows 3 and 4 show shoulder and elbow kinematics. Keys: PEC, pectoralis m.; P.DEL, posterior deltoid m.; BIC, biceps m.; TRI, triceps m.; Θ_s, shoulder joint position; $\dot{\Theta}_s$, shoulder joint velocity; Θ_e, elbow joint position; $\dot{\Theta}_e$, elbow joint velocity.
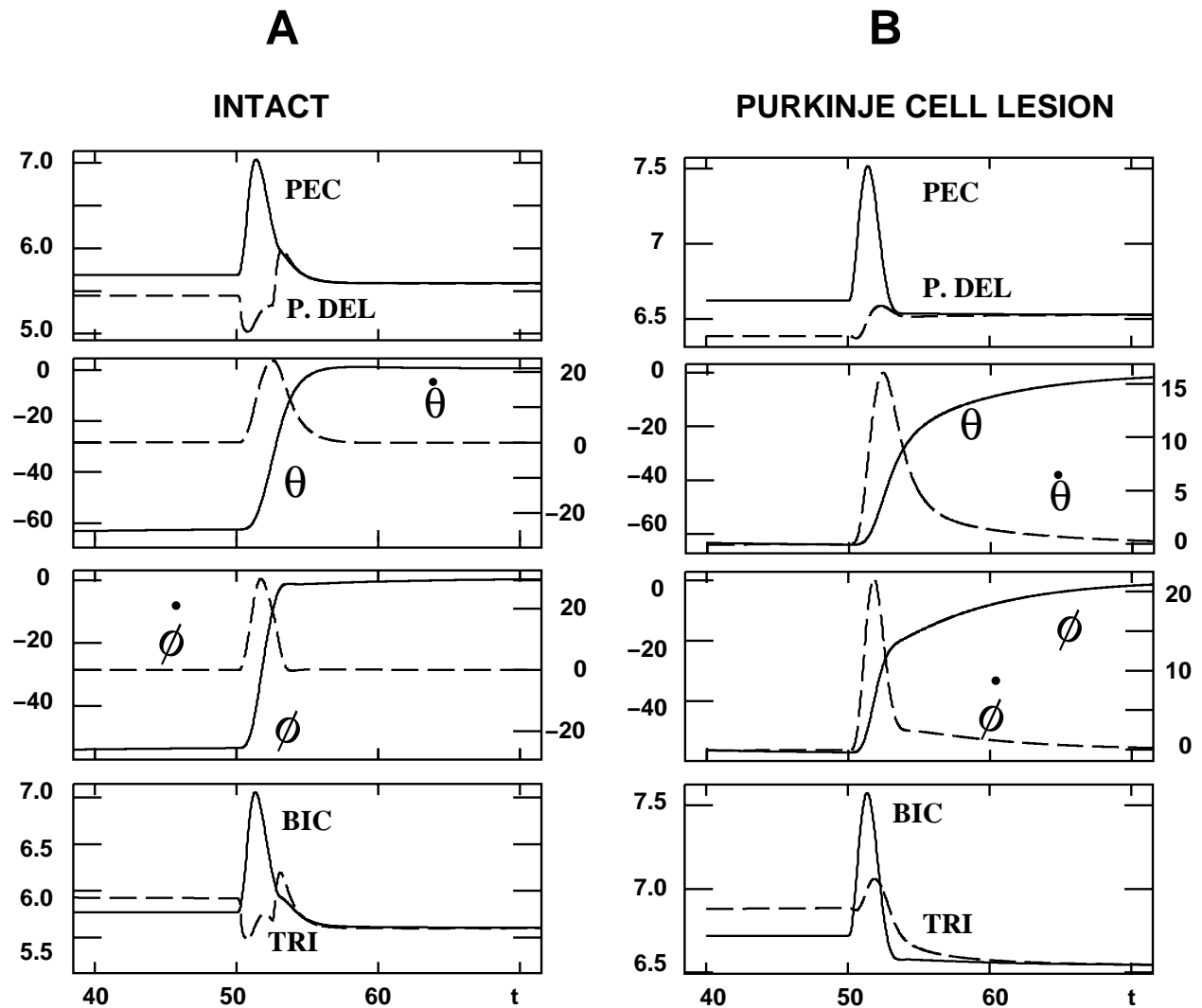
Figure 13: Simulation of the dynamics of the 2D planar VITE-FLETE-CEREBELLUM system for (A) the intact system and (B) when the cerebellar cortex is damaged (e.g. Purkinje cells no longer inhibit NIP cells). Plots show simulated joint position and velocity for shoulder $(\Theta, \dot{\Theta})$ and elbow $(\Theta, \dot{\Theta})$ joints, as well as simulated α motoneuron activities. The Purkinje cell output lesion removes phasic cerebellar disinhibition of NIP cells, while also tonically disinhibiting them. This results in higher peak values, reduced ranges, and higher baseline levels of α-MN activity, as well as coactivation of antagonist muscles. The trajectories for the Purkinje-lesioned system show decreased rise times and increased settling times.

The plots of joint position and velocity of Figure 13B show that the movement evolves slower compared to the intact system simulation shown in panel A. The α-MN activities show a higher baseline of activities which is correlated with the higher level of tonic NIP output (Figure 14) resulting from removal of Purkinje cell inhibition. Note also that the antagonist motoneuron pool is not inhibited during the early part of the movement and that the antagonist braking bursts are smaller in amplitude. Figure 14 shows that in the NIP only an agonist burst is generated, albeit of different duration, due to the corollary discharge from mossy fibers from the agonist channel. However, the amplitude of the agonist NIP response is reduced in amplitude after the cerebellar cortex lesion.

These simulations suggest that the cerebellar cortex plays an important role in modulating interpositus nuclear cell discharge, so as to facilitate the initiation and performance of limb movements. In summary, a simulated lesion in the model's cerebellar cortex, without damaging the deep nuclei shows that although motor performance is degraded, arm movements are still performed, albeit with a slower time course and impaired regularity or smoothness.
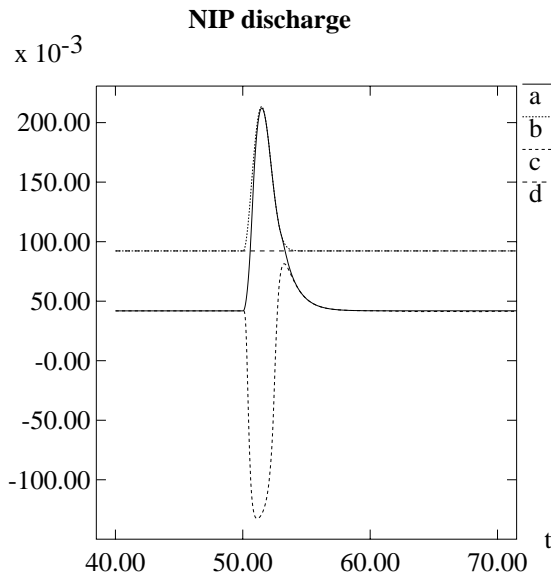
Figure 14: Interpositus nuclei cell discharge for the agonist and antagonist channels before (a:agonist, b:antagonist) Purkinje cell lesion; and after Purkinje cell lesion (c:agonist, d:antagonist). After the Purkinje cell lesion, the baseline of activity of NIP cells increases due to Purkinje cell disinhibition, the duration of the agonist NIP burst is shorter, and no antagonist burst is generated in the other NIP pool.

4   Conclusions

An adaptive, context-dependent, preemptive error reduction mechanism has been proposed to model cerebellar control of descending motor commands and tuning of proprioceptive reflexes during multijoint movements. Specifically, the cerebellar model uses muscle-specific discrete error signals from the inferior olive and nonspecific parallel fiber signals from

granule cells to learn weight distributions that improve inverse dynamic computations on a trial-by-trial basis.

It is hypothesized that LTD of parallel fiber-Purkinje cell synapses, induced by conjunctive stimulation of parallel fiber and climbing fiber, and LTP of parallel fiber-Purkinje cell synapses, induced by repetitive stimulation of parallel fibers alone, can lead to the discovery of opponent muscle synergies by cerebellar circuitry, which enables efficient opponent multi-joint muscle control. It is shown that the only requirement for opponent cerebellar control is the specificity of climbing fiber projections from the inferior olive to both the cerebellar cortex and deep nuclear zones that project back through the rubral-spinal tract to control the same muscles that provide afferent inputs to specific inferior olivary zones. Thus the model incorporates findings indicating that topographical order is maintained through circuits that traverse the olive and associated deep nuclear zones, and shows that this design produces adaptive results when extended to include appropriate somatosensory feedback, in this case from stretch receptors.

Large-scale simulations of the cerebellar model in interaction with an arm movement cortical central pattern generator and a spinal force controller show that: (1) mossy fiber conduction of movement velocity commands from the CPG to both the cerebellar cortex and associated nucleus NIP/RN leads to generation of phasic nuclear cell responses whose feedforward action can greatly improve upon spinal feedback control of tracking, including reduction of oscillations; and (2) phasic NIP/RN excitation of motoneurons, coupled with phasic inhibition of the Renshaw cells associated with those motoneurons, yields better tracking than either operation alone. These results help explain the need for the dual spinal level action of rubral stimulation that was discovered by Henatsch *et al.*, (1986).

Other influences of the cerebellar-rubral pathway in spinal circuitry

Besides reports of direct monosynaptic rubro-motoneuronal connections to the cat's forelimb motoneurons, particularly in the C8-T1 segments (Fujito, Imani and Aoki, 1991), and differential effects of stimulation of the cat's red nucleus on lumbar alpha motoneurons and their Renshaw cells (Henatsch *et al.*, 1986), Hongo, Jankowska and Lundberg (1972b) have shown that stimulation of the red nucleus produces monosynaptic excitatory effects on cells monosynaptically activated, or disynaptically inhibited, from group I muscle afferents and in cells di- or polysynaptically activated from the flexor reflex afferents or exclusively from cutaneous afferents. Hongo *et al.*, (1972a) demonstrated that stimulation of the RN evokes a large dorsal root potential followed by pronounced primary afferent depolarizations in Ib and low threshold cutaneous afferents, and a dual effect on Ia afferent terminals. These mono-synaptic effects on Ia afferents or IaINs could contribute to the cerebellar tuning of proprioceptive reflexes and other control loops through changes in the organization, gain and timing of these reflexes. These effects may be explained using modest extensions to the model proposed in Figure 2, through a more complete analysis of how NIP/RN outputs to spinal cord affect the processing of sensory feedback during arm movement control.

Comparison with other cerebellar models

Grossberg and Kuperstein (1986) developed a model of error-based opponent learning of adaptive gain control by the cerebellum. This work built on Grossberg's (1969) cerebellar model, which suggested that both LTD and LTP occurred at the parallel fiber-Purkinje cell synapse to learn to control linearly ordered motor components. The early

cerebellar model of Marr (1969) assumed that only LTP occurred, whereas that of Albus (1971) invoked LTD at parallel fiber synapses with both Purkinje and stellate cells to allow bi-directional weight changes. Smith (1981) proposed how the cerebellar connectivity could allow for agonist-antagonist opponent muscle control. He hypothesized that during cocontraction of antagonist muscles, afferents from each opponent muscle converge on cerebellar inhibitory interneurons to remove the Purkinje cell inhibition of the deep cerebellar nuclei. Furthermore, Smith suggested that by inhibiting groups of deep nuclear cells, Purkinje cells could mediate disfacilitation of motoneuron pools resulting in antagonist muscle relaxation. Recently, Smith (1996) proposed that pairs of Purkinje cells, as in our model and that of Grossberg and Kuperstein (1986), could use reciprocal inhibition or antagonist cocontraction to control agonist-antagonist muscle groups. These models are compatible with the idea that the cerebellum is involved in the learning and coordination of muscle synergies (Thach, 1992). Moreover, these models work under the assumption that the command for movement originates outside the cerebellum, that this command provides a reference for computing error feedback signals, and that the cerebellar output projections to the spinal centers (e.g. the rubrospinal tract) form a side-path with respect to the descending cortico-spinal motor pathways (Ito, 1984). This is in contrast to models that postulate the cerebellum as an adjustable pattern generator (e.g., Houk *et al.*, 1993) responsible for primary trajectory generation.

Our opponent cerebellar model for arm movement control considerably extends Smith's (1981, 1996) proposal by demonstrating how an afferent pattern suitable for regulating cocontraction or reciprocal inhibition of antagonist muscles can be established by learning due to the spatiotemporal correlation at Purkinje of mossy and climbing fiber discharges in the same, but not in opposing or unrelated, channels. This cerebellar learning hypothesis places few demands on a-priori wiring for control of opponency in the cerebellum, and extends to controlling a large number of muscles acting at several joints. As such, this competence appears to be beyond what can be accomplished by the segmental organizational scheme utilized by spinal stretch reflexes unassisted by learned descending modulation. In fact, the proposed cerebellar model allows a generalization of rapid, and in that sense reflex-like, control beyond the one-joint, two-muscle level of organization (Bullock *et al.*, 1993b; Thach *et al.*, 1992).

5   Appendix A: Simulation methods

All simulations were performed using the classic Runge-Kutta fourth-order method or the Runge-Kutta-Nyström method (Collatz, 1966). Simulations were performed by integrating the dynamical system that defines the model described in the Methods section. The simulations were started with all the system's variables initially set to 0.0, except for the PF-PC connectivity matrix which was set to the identity matrix.

For a typical single joint VITE-FLETE-CEREBELLUM simulation, the following equations were integrated: Equations (1)–(3) for VITE, Equations (4)–(29) for FLETE, and Equations (32)–(39) for the cerebellar model. The inputs variables were: G_0, Go signal multiplier; the target position vector (T_1, T_2), P the coactivation signal, and the output variables were joint position (Θ) and velocities $(\dot{\Theta})$, muscle forces (F_1, F_2), α-MN activities (M_1, M_2) and spindle feedback (E_1, E_2).

For the 2D simulations, we used Equations (1)–(3) for each of the two VITE systems (one for each limb segment), Equations (4)–(5), (9)–(31), and (40)–(51) for each FLETE system controlling the shoulder and the elbow joints, and Equations (32)–(36), (38)–(39) for the cerebellar model extended to the 2D case using the connectivity matrix depicted in Figure 10. As in the single joint simulation, the input variables were: G_0, Go signal multiplier; the target position vector (T_1, T_2) for each VITE; Go signal multiplier common to both VITE systems; and the output variables were shoulder and elbow joint position (Θ and Φ respectively) and shoulder and elbow joint velocities ($\dot{\Theta}$ and $\dot{\Phi}$ respectively), muscle forces (F_1, F_2), for the shoulder and elbow; and α-MN activities (M_1, M_2) for the shoulder and elbow MN pools. Note that as the moment arm was set equal to 1.0, the shoulder and elbow torque variables in Equations (40)–(41) corresponded actually to the difference between agonist and antagonist muscle forces for the shoulder (Equation (40)) and elbow (Equation (41)) joints. Also gravity was neglected as the simulations involved horizontal planar arm movements.

6 References

Reference

Akazawa, K. and Kato, K. (1990). Neural network model for control of muscle force based on the size principle of motor unit. *Proceedings of the IEEE*, **78**, 1531–1535.

Albus, J.S. (1971). A theory of cerebellar function. *Mathematical Biosciences*, **10**, 25–61.

Alexander, R.M. (1981). Mechanics of skeleton and tendons. In: **Handbook of Physiology. The Nervous System. Motor Control.** Bethesda, MD: American Physiology Society, Sec. 1, Vol. II, part 1, 17–42.

Anderson, R.A. (1987). Inferior parietal lobule function in spatial perception and visuomotor integration. In F. Plum, V.B. Mountcastle, and S.R. Geiger (Eds.), **Handbook of physiology, Section 1: The nervous system, Volume V**. Higher functions of the brain, Part 2. Bethesda, MD: American Physiological Society, 483–518.

Araki, T., Eccles, J.C. and Ito, M. (1960). Correlation of the inhibitory postsynaptic potential of motoneurones with the latency and time course of inhibition of monosynaptic reflexes. *Journal of Physiology* (London), **154**, 354–377.

Asada, H. and Slotine, J.J. E. (1986). **Robot Analysis and Control**. New York:Wiley-Interscience.

Baldissera, F., Cavallari, P., Fournier, E., Pierrot-Deseilligny, E., and Shindo, M. (1987). Evidence for mutual inhibition of opposite Ia interneurones in the human upper limb. *Experimental Brain Research*, **66**, 106–114.

Bartha, G.T., Thompson, R.F., and Gluck, M.A. (1991). Sensorimotor learning and the cerebellum. In: M. Arbib and J. Ewert (Eds.), **Visual Structures and Integrated Functions**. Berlin:Springer-Verlag, 381–396.

Bloedel, J.R. and Bracha, V. (1995). On the cerebellum, cutaneomuscular reflexes, movement and the elusive engrams of memory. *Behavioral Brain Research*, **68**, 1–44.

Bloedel, J.R., and Courville, J. (1981). Cerebellar afferent systems. In: *Handbook of Physiology. The Nervous System. Motor Control.* Bethesda, MD: American Physiology Society, Sec. 1, Vol. II, part 2, 735–829.

Brink, E., Jankowska, E., McCrea, D.A., and Skoog, B. (1983). Inhibitory interactions between interneurones in reflex pathways from group Ia and group Ib afferents in the cat. *Journal of Physiology* (London), **343**, 361–373.

Bullock, D., Cisek, P., Grossberg, S. (1997). Cortical networks for control of voluntary movements under variable force conditions. Technical Report CAS/CNS-TR-95-019. Boston, MA: Boston University. *Cerebral Cortex*, in press.

Bullock, D. and Contreras-Vidal, J.L. (1993). How spinal neural networks reduce discrepancies between motor intention and motor realization. In K. Newell and D. Corcos (Eds.), **Variability and motor control**, Champaign, Illinois: Human Kinetics Press, 183–221.

Bullock, D., Contreras-Vidal, J.L., and Grossberg, S. (1993a). Speed scaling and adaptive cerebellar control of Renshaw cell and motoneuron gain. *Society for Neuroscience Abstracts*, **19**, Part 2, 655.6, 1594.

Bullock, D., Contreras-Vidal, J.L., and Grossberg, S. (1993b). Cerebellar learning in an opponent motor controller for adaptive load compensation and synergy formation. In: *Proceedings of the World Congress on Neural Networks*, **IV**, 481–486.

Bullock D., Contreras-Vidal, J.L., and Grossberg, S. (1993c). Equilibria and dynamics of a neural network for opponent muscle control. In G.A. Bekey and K.Y. Goldberg (Eds.), **Neural networks in robotics**. Boston, MA: Kluwer Publishing, 439–457.

Bullock, D., Fiala, J.C., and Grossberg, S. (1994). A neural model of timed response learning in the cerebellum. *Neural Networks*, **7**, 1101–1114.

Bullock, D. and Grossberg, S. (1988). Neural dynamics of planned arm movements: Emergent invariants and speed-accuracy properties during trajectory formation. *Psychological Review*, **95**, 49–90.

Bullock, D. and Grossberg, S. (1989). VITE and FLETE: Neural modules for trajectory formation and tension control. In W. Hershberger (Ed.), **Volitional Action**. Amsterdam: North-Holland, 253–297.

Bullock, D. and Grossberg, S. (1991). Adaptive neural networks for control of movement trajectories invariant under speed and force rescaling. *Human Movement Science*, **10**, 3–53.

Bullock, D. and Grossberg, S. (1992). Emergence of tri-phasic muscle activation from the nonlinear interactions of central and spinal neural network circuits. *Human Movement Science*, **11**, 157–167.

Burbaud, P., Doegle, C., Gross, C., and Bioulac, B. (1991). A quantitative study of neuronal discharge in areas 5, 2, and 4 of the monkey during fast arm movements. *Journal of Neurophysiology*, **66**, 429–443.

Burgess, P.R., Wei, J.Y., Clark, F.K., and Simon, J. (1982). Signaling of kinesthestic information by peripheral sensory receptors. *Annual Review of Neuroscience*, **5**, 171–187.

Carli, G., Farabollini, F.. Fontani, G., and Meucci, M. (1979). Slowly adapting receptors in cat hip joint. *Journal of Neurophysiology*, **39**, 767–778.

Chapman, C.E., Spidalieri, G., and Lamarre, Y. (1984). Discharge properties of area 5 neurones during arm movements triggered by sensory stimuli in the monkey. *Brain Research*, **309**, 63–77.

Cisek, P., Grossberg, S., and Bullock, D. (1996). A cortico-spinal model of reaching and proprioception under multiple task constraints. Technical Report CAS/CNS-TR-96-035. Boston, MA: Boston University.

Collatz, L. (1966). **The Numerical Treatment of Differential Equations**. Third Edition, New York: Springer-Verlag.

Contreras-Vidal, J.L. (1994). Neural networks for motor learning and regulation of posture and movement. Ph.D. Dissertation at Boston University. Ann Arbor, MI: UMI, Number 9334218.

Contreras-Vidal, J.L., and Stelmach, G.E. (1995). A neural model of basal ganglia-thalamocortical relations in normal and parkinsonian movement, *Biological Cybernetics*, **73**, 467–476.

Courville, J., Augustine, J.R., and Martel, P. (1977). Projections from the inferior olive to the cerebellar nuclei in the cat demonstrated by retrograde transport of horseradish peroxidase, *Brain Research*, **130**, 405–419.

Crammond, D.J. and Kalaska, J.F. (1989). Neuronal activity in primate parietal cortex area 5 varies with intended movement direction during an instructed-delay period. *Experimental Brain Research*, **76**, 458–462.

Crepel, F., Hemart, N., Jaillard, D., and Daniel, H. (1996). Cellular mechanisms of long-term depression in the cerebellum. *Behavioral and Brain Sciences*, **19**, 347–353.

DeLuca, C.J. (1985). Control properties of motor units. *Journal of Experimental Biology*, **115**, 125–136.

Dum, R.P., and Strick, P.L. (1990). Premotor areas: Nodal points for parallel efferent systems involved in the central control of movement. In D.R. Humphrey and D.R. Freund (Eds.), **Motor control: concepts and issues**. London: Wiley, 383–397.

Eccles, J. (1977). An instruction-selection theory of learning in the cerebellar cortex. *Brain Research*, **127**, 327–352.

Eccles, J.C., Eccles, R.M., and Lundberg, A. (1957). The convergence of monosynaptic excitatory afferents on to many different species of alpha motoneurons. *Journal of Physiology*, **137**, 22–50.

Eccles, J.C., Faber, D.S., Murphy, J.T., Sabah, N.H., and Táboříková, H. (1971a). Afferent volleys in limb nerves influencing impulse discharges in cerebellar cortex. I. In mossy fibers and granule cells. *Experimental Brain Research*, **13**, 15–35.

Eccles, J.C., Faber, D.S., Murphy, J.T., Sabah, N.H., and Táboříková, H. (1971b). Afferent volleys in limb nerves influencing impulse discharges in cerebellar cortex. II. In purkinje cells. *Experimental Brain Research*, **13**, 36–53.

Eccles, J.C., Fatt, P., and Koketsu, K. (1954). Cholinergic and inhibitory synapses in a pathway from motor-axon collaterals to motorneurones. *Journal of Physiology* (London), **126**, 524–562.

Eccles, J.C. Ito, M. and Szentágothai, J. (1967). **The Cerebellum as a Neuronal Machine**. New York:Springer-Verlag.

Eccles, R.M., and Lundberg, A. (1958). Integrative pattern of Ia synaptic actions on motoneurons of hip and knee muscles. *Journal of Physiology* (London), **144**, 271–298.

Ellaway, P.H. (1968). Antidromic inhibition of fusimotor neurones. *Journal of Physiology* (London), **198**, 39P–40P.

Ellaway, P.H. and Murphy, P.R. (1980). A quantitative comparison of recurrent inhibition of α and γ-motoneurones in the cat. *Journal of Physiology* (London), **315**, 43–58.

Ellias, S.A. and Grossberg, S. (1975). Pattern formation, contrast control, and oscillations in the short term memory of shunting on-center off-surround networks. *Biological Cybernetics*, **20**, 69–98.

Fiala, J.C. and Bullock, D. (1996). Timing implications of metabotropic mechanisms for cerebellar learning. *Behavioral and Brain Sciences*, **19**, 445–447.

Fiala, J.C., Grossberg, S., and Bullock, D. (1996). Metabotropic glutamate receptor activation in cerebellar Purkinje cells as substrate for adaptive timing of the classically conditioned eye blink response. *Journal of Neuroscience*, **16**, 3760–3774.

Fromm, C., Wise, S.P., and Evarts, E.V. (1984). Sensory response properties of pyramidal tract neurons in the precentral motor cortex and postcentral gyrus of the rhesus monkey. *Experimental Brain Research*, **54**, 177–185.

Fujito, Y., Imai, T., and Aoki, M. (1991). Monosynaptic excitation of motoneurons innervating forelimb muscles following stimulation of the red nucleus in cats. *Neuroscience Letters*, **127**, 137–140.

Georgopoulos, A.P., Kalaska, J.F., Caminiti, R., and Massey, J.T. (1982). On the relations between the direction of two-dimensional arm movements and cell discharge in primate motor cortex. *Journal of Neuroscience*, **2**, 1527–1537.

Gibson, A.R., Houk, J.C., and Kohlerman, N.J. (1985). Relation between red nucleus discharge and movement parameters in trained macaque monkeys. *Journal of Physiology*, **358**, 551–570.

Grossberg, S. (1969). On learning of spatiotemporal patterns by networks with ordered sensory and motor components, I. Excitatory components of the cerebellum. *Studies in Applied Mathematics*, **48**, 105–132.

Grossberg, S., and Kuperstein, M. (1986). **Neural dynamics of adaptive sensory-motor control**. Elmsford, N.Y. Pergamon Press.

Henatsch, H.D., Meyer-Lohmann, J., Windhorst, U., and Schmidt, J. (1986). Differential effects of stimulation of the cat's red nucleus on lumbar alpha motoneurones and their Renshaw cells. *Experimental Brain Research*, **62**, 161–174.

Henneman, E. (1957). Relation between size of neurons and their susceptibility to discharge. *Science*, **26**, 1345–1347.

Henneman, E. (1985). The size-principle: A deterministic output emerges form a set of probabilistic connections. *Journal of Experimental Biology*, **115**, 105–112.

Hirano, T. (1990). Depression and potentiation of the synaptic transmission between a granule cell and a purkinje cell in rat cerebellar culture. *Neuroscience Letters*, **119**, 141–144.

Hirano, T. (1991). Differential pre- and postsynaptic mechanisms for synaptic potentiation and depression between a granule cell and a purkinje cell in rat cerebellar culture. *Synapse*, **7**, 321–323.

Hongo, T., Jankowska, E., and Lundberg, A. (1972a). The rubrospinal tract III. Effects on primary afferent terminals. *Experimental Brain Research*, **15**, 39–53.

Hongo, T., Jankowska, E., and Lundberg, A. (1972b). The rubrospinal tract IV. Effects on interneurons. *Experimental Brain Research*, **15**, 54–78.

Horak, F.B. and Anderson, M.E. (1984a). Influence of globus pallidus on arm movements in monkeys. I. Effects of kainic acid-induced lesions. *Journal of Neurophysiology*, **52**, 290–304.

Horak, F.B. and Anderson, M.E. (1984b). Influence of globus pallidus on arm movements in monkeys. II. Effects of stimulations. *Journal of Neurophysiology*, **52**, 305–322.

Hore J., Wild B., and Diener H.C. (1991). Cerebellar dysmetria at the elbow, wrist and fingers. *Journal of Neurophysiology*, **65**, 563–571.

Houk, J.C., Keifer, J., and Barto, A.G. (1993). Distributed motor commands in the limb premotor network. *Trends in Neurosciences*, **16**, 27–33.

Houk, J.C., Singh, S.P., Fisher, C., and Barto, A.G. (1990). An adaptive sensorimotor network inspired by the anatomy and physiology of the cerebellum. In: Miller, W.T., Sutton, R.S., Werbos, P.J. (Eds.) **Neural Networks for Control**. Ch. 13. Cambridge, Mass., MIT Press, 301–348.

Hultborn, H., Jankowska, E., Lindström, S. (1971). Recurrent inhibition of interneurons monosynaptically activated from group Ia afferents. *Journal of Physiology* (London), **215**, 613–636.

Hultborn, H., Illert, M., and Santini, M. (1976). Convergence on interneurones mediating the reciprocal *Ia* inhibition of motoneurons I. Disynaptic *Ia* inhibition of *Ia* inhibitory interneurones. *Acta Physiology Scand.*, **96**, 193–201.

Hultborn H., Lindström, S., and Wigstrom, H. (1979). On the function of recurrent inhibition in the spinal cord. *Experimental Brain Research* **37**, 399–403.

Humphrey, D.R. and Reed, D.J. (1983). Separate cortical systems for control of joint movement and joint stiffness: Reciprocal activation and coactivation of antagonist muscles. In J.E. Desmedt (Ed.), **Motor control mechanisms in health and disease**. New York: Raven Press, 347–372.

Ito, M. (1984). **The cerebellum and neural control**. New York: Raven.

Ito, M. (1991). The cellular basis of cerebellar plasticity. *Current Opinions in Neurobiology*, **1**, 616–620.

Ito, M. and Karachot, L. (1992). Protein kinases and phosphatase inhibitors mediating long-term desensitization of glutamate receptors in cerebellar Purkinje cells. *Neuroscience Research*, **14**, 27–38.

Ito, M., Yoshida, M. (1966). The origin of cerebellar-induced inhibition of Deiters' neurons. I. Monosynaptic initiation of the inhibitory postsynaptic potentials, *Experimental Brain Research*, **2**, 330–349.

Ito, M., Yoshida, M., Obata, K., Kawai, N., and Udo, M. (1970). Inhibitory control of intracerebellar nuclei by the Purkinje cell axons. *Experimental Brain Research*, **10**, 64–80.

Kano, M. (1996). A bridge between cerebellar long-term depression and discrete motor learning: Studies on gene knockout mice. *Behavioral and Brain Sciences*, **19**, 488–490.

Kalaska, J.F., Cohen, D.A.D., Hyde, M.L., and Prud'homme, M.J. (1989). A comparison of movement direction-related versus load direction-related activity in primate motor cortex, using a two-dimensional reaching task. *Journal of Neuroscience*, **9**, 2080–2102.

Kalaska, J.F., Cohen, D.A.D., Prud'homme, M.J., and Hyde, M.L. (1990). Parietal area 5 neuronal activity encodes movement kinematics, not movement dynamics. *Experimental Brain Research*, **80**, 351–364.

Karst, G.M. and Hasan, Z. (1991). Initiation rules for planar, two-joint arm movements: Agonist selection for movements throughout the work space. *Journal of Neurophysiology*, **66**, 1579–1593.

Kato, M. and Kimura, M. (1992). Effects of reversible blockade of basal ganglia on a voluntary arm movement. *Journal of Neurophysiology*, **65**, 1516–1534.

Kawato, M. and Gomi, H. (1991). A computational model of four regions of the cerebellum based on feedback-error learning. *Biological Cybernetics*, **68**, 95–103.

Kettner, R.E., Schwartz, A.B., and Georgopoulos, A.P. (1988). Primate motor cortex and free arm movements to visual targets in three-dimensional space. III. Positional gradients and population coding of movement direction from various movement origins. *Journal of Neuroscience*, **8**, 2938–2947.

Kirsch, R.F. and Rymer, W.Z. (1987). Neural compensation for muscular fatigue: Evidence for significant force regulation in man. *Journal of Neurophysiology*, **57**, 1893–1910.

Lacquaniti, F., Guigon, E., Bianchi, L., Ferraina, S., and Caminiti, R. (1995). Representing spatial information for limb movement: Role of area 5 in the monkey. *Cerebral Cortex*, **5**, 391–409.

Laporte, Y. and Lloyd, D.P.C. (1952). Nature and significance of the reflex connections established by large afferent fibers of muscular origin. *American Journal of Physiology*, **169**, 609–621.

Lestienne, F. (1979). Effects of inertial load and velocity on the braking process of voluntary limb movements. *Experimental Brain Research*, **35**, 407–418.

Llinás, R. (1981). Electrophysiology of the cerebellar networks. In: *Handbook of physiology. The nervous system. Motor control.* Bethesda, MD: American Physiology Society, Sec. 1, Vol. II, part 2, 831–876.

Llinás, R., Baker, R., and Sotelo, C. (1974). Electrotonic coupling between neurons in cat inferior olive. *Journal of Neurophysiology,* **37**, 560–571.

Llinás, R. (1989). Electrophysiological properties of the olivocerebellar system. In P. Strata (Ed.), **The Olivocerebellar System in Motor Control.** New York: Springer-Verlag, 201–208.

Lloyd, D.P.C. (1943). Conduction and synaptic transmission of the reflex response to stretch in spinal cats. *Journal of Neurophysiology*, **6**, 317–326.

Mano, N., Kanazawa, I., and Yamamoto, K. (1989). Voluntary movements and complex-spike discharges of cerebellar purkinje cells. In P. Strata (Ed.). **The olivocerebellar system in motor control.** New York: Springer-Verlag, 265–280.

Marr, D. (1969). A theory of cerebellar cortex. *Journal of Physiology*, London, **202**, 437–470.

Martin, J.H. and Ghez, C. (1991). Task-related coding of stimulus and response in cat red nucleus. *Experimental Brain Research*, **85**, 373–388.

Matthews, P.B.C. (1981). Review lecture: Evolving views on the internal operation and functional role of the muscle spindle. *Journal of Physiology* (London), **320**, 1–30.

Miall, R.C., Malkmus, M., and Robertson, E.M. (1996). Sensory prediction as a role for the cerebellum. *Behavioral and Brain Sciences*, **19**, 466–467.

Millar, J. (1975). Flexion-extension sensitivity of elbow joint afferents in cat. *Experimental Brain Research*, **24**, 209–214.

Nagasaki, H. (1989). Asymmetric velocity and acceleration profiles of human arm movements. *Experimental Brain Research*, **74**, 319–326.

Renshaw, B. (1941). Influence of discharge of motoneurones upon excitation of neighboring motoneurons. *Journal of Neurophysiology*, **4**: 167–183.

Renshaw, B. (1946). Central effects of centripetal impulses in axons of spinal ventral roots. *Journal of Neurophysiology*, **9**, 191–204.

Robinson, C.J. and Burton, H. (1980). Organization of somatosensory receptive fields in cortical areas 7b, retroinsular postauditory and granular insula of M. fascicularis. *Journal of Comparative Neurology*, **192**, 69–92.

Robison, F.R., Houk J.C., and Gibson, A.R. (1987). Limb specific connections of the cat magnocellular red nucleus. *Journal of Comparative Neurology*, **257**, 553–577.

Ryall, R.W. (1970). Renshaw cell mediated inhibition of Renshaw cells: Patterns of excitation and inhibition from impulses in motor axon collaterals. *Journal of Neurophysiology*, **33**, 257–270.

Ryall, R.W., and Piercey, M. (1971). Excitation and inhibition of Renshaw cells by impulses in peripheral afferent nerve fibers. *Journal of Neurophysiology*, **34**, 242–251.

Sakurai, M. (1987). Synaptic modification of parallel fiber-Purkinje cell transmission in the in vitro guinea pig cerebellar slices. *Journal of Physiology* (London), **394**, 463–480.

Shinoda, Y., Sugiuchi,Y., Futami, T., and Izawa, R. (1992). Axon collaterals of mossy fibers from the pontine nucleus in the cerebellar dentate nucleus. *Journal of Neurophysiology*, **67**, 547–560.

Smith, A.M. (1981). The coactivation of antagonist muscles, *Canadian Journal of Physiology and Pharmacology*, **59**, 733–747.

Smith A.M. (1996). Does the cerebellum learn strategies for the optimal time-varying control of joint stiffness? *Behavioral and Brain Sciences*, **19**, 399–410.

Stein J.F. and Glickstein M. (1992). The role of the cerebellum in the visual guidance of movement. *Physiological Review*, **72**, 967–1017.

Thach W.T., Goodkin H.P., and Keating J.G. (1992). The cerebellum and the adaptive coordination of movement, *Annual Review Neuroscience*, **15**, 403–442.

Tracey, D.J. (1979). Characteristics of wrist joint receptors in the cat. *Experimental Brain Research*, **34**, 165–176.

Zatsirosky, V. and Seluyanov, D. (1983). The mass and inertia characteristics of the main segments of the human body. In H. Matsui and K. Kobayashi (Eds.), **Biomechanics VIIIB**. Champaign, IL: University Park Press, 1152–1159.